CRISPR-Cas9 Screens Reveal Genes Regulating a G0-like State in Human Neural Progenitors

Heather M. Feldman[1], Chad M. Toledo[1,2], Sonali Arora[1], Pia Hoellerbauer[1,2], Philip Corrin[1], Lucas Carter[1], Megan Kufeld[1], Hamid Bolouri[1], Ryan Basom[3], Jeffrey Delrow[3], Joshua Meier[4], Feng Zhang[4], José L. McFaline-Figueroa[5], Cole Trapnell[5], Steven M. Pollard[6], Christopher L. Plaisier[7]* and Patrick J. Paddison[1,2]*

[1]Human Biology Division, Fred Hutchinson Cancer Research Center, Seattle, WA, USA 98109; [2]Molecular and Cellular Biology Program, University of Washington, Seattle, WA, USA 98195; [3]Genomics and Bioinformatics Shared Resources, Fred Hutchinson Cancer Research Center, Seattle, WA, USA 98109;[4]Department of Brain and Cognitive Sciences and Biological Engineering, Massachusetts Institute of Technology, Cambridge, MA, USA 02139; [5]Department of Genome Sciences, University of Washington, Seattle, WA, USA 98195; [6]Edinburgh CRUK Cancer Research Centre and MRC Centre for Regenerative Medicine, The University of Edinburgh, Edinburgh, UK EH16 4UU; [7]School of Biological and Health Systems Engineering, Arizona State University, Tempe, AZ, USA 85281.

*To whom correspondence should be addressed: Christopher Plaisier (plaisier@asu.edu) or Patrick Paddison (paddison@fredhutch.org).

***Running title**:* Regulation of G0-like State in hNPCs

Abstract

The coordination of developmental potential and proliferation in stem and progenitor cells is essential for mammalian development and tissue homeostasis. We performed CRISPR-Cas9 screens in human neural progenitor cells (hNPCs) and identified genes, including *CREBBP*, *NF2*, *PTPN14*, *TAOK1*, or *TP53*, that limit expansion. Knockout of these genes causes increased hNPC proliferation via skipping of a transient G0-like state, characterized by expression of genes associated with quiescent neural stem cells and neural development and molecular features of quiescent cells (e.g., hypophosphorylated Rb, low CDK2 activity, and p27 stabilization). Single-cell RNA-sequencing of hNPCs revealed distinct G0/G1 populations, altered in G0-skip mutants through both distinct and convergent downstream effectors, including cell cycle, Hippo-YAP, and novel targets. Our results provide a molecular and phenotypic portrait of expanding hNPCs including a gene expression map of their cell cycle and characterization of antiproliferative factors that regulate cell cycle exit with likely roles in maintaining developmental potential.

Key words: CRISPR-Cas9/G0/human neural progenitor cells/quiescence/scRNA-sequencing

Introduction

In mammals, most developing and adult tissues are hierarchically organized such that tissue growth and maintenance is driven by the production of lineage-committed cells from populations of tissue-resident stem and progenitor cells (Reya, Morrison et al., 2001). In adult tissues, stem cells are typically found in a quiescent or reversible G0 state, but must re-enter the cell cycle and divide to promote lineage commitment (Doetsch, 2003, Obernier, Cebrian-Silla et al., 2018). Their lineage committed progeny, e.g., amplifying progenitors, further balance lineage potential with proliferation to produce enough terminally differentiated cells to keep pace with demand (Lin, 2008). This balance of proliferation and self-preservation is particularly crucial for neural progenitor cells which cannot compensate for differences in cell number by altering cell size due to the functional requirements of the resulting neural networks (Homem, Repic et al., 2015). Thus disruption of the balance between self-renewal and proliferation during development may lead to severe defects in brain architecture, such as microcephaly or megacephaly (Homem et al., 2015).

Neural progenitor cells (NPCs) derived from the developing mammalian telencephalon (Davis & Temple, 1994, Johe, Hazel et al., 1996) can be cultured *ex vivo* yet recapitulate the expansion, specification, and maturation of each of the major cell types in the mammalian central nervous system. When grown in defined, serum-free conditions *in vitro* in the presence of epidermal and fibroblast growth factors (EGF and FGF), these cells retain progenitor-like molecular features, including Nestin and Sox2 expression, and capacity for multi-lineage differentiation (Pollard, Conti et al., 2006, Sun, Pollard et al., 2008). As such, these cells represent a model for both

understanding basic stem/progenitor cell biology and a tractable system for functional genomics to uncover the regulatory pathways that maintain the precise regulation of cell cycle exit.

Here, we identify genes that govern the self-renewal and proliferation of hNPCs *in vitro* by CRISPR-Cas9 genome-wide screening for genes rate-limiting for expansion. We found that knock-out (KO) of five genes, *CREBBP*, *NF2*, *PTPN14*, *TAOK1*, or *TP53*, all known or candidate tumor suppressors, robustly increased hNPC expansion as a result of shortening G1 phase and, more specifically, skipping a transient G0-like state of variable length.

In-depth characterization and analysis of hNPCs using single-cell RNA-sequencing revealed four definable G0/G1 populations, which are altered in G0-skip mutants. In particular, we observe that the G0-skip mutants promote expansion of a late G1 population enriched in key cell cycle regulators (e.g., *MYC*, *CCND1*) and Hippo-YAP targets at the expense of a G0-like subpopulation enriched for expression of neurodevelopment genes and those found in quiescent NSCs (e.g., *CLU*, *HOPX*). Further, characterization of G0/G1-specific gene expression for each G0-skip gene KO yielded a rich data resource for analysis of the p53 transcriptional network, Hippo-YAP targets, cell cycle gene regulation, and many novel targets and pathways, including those downstream of CREBBP and TAOK1. The results suggest that hNPC expansion is constrained by a transient G0-like state, regulated by multiple pathways, that facilitates retention of neurodevelopmental identity.

RESULTS

CRISPR-Cas9 gene knockout screens identify antiproliferative genes in hNPCs

To identify proliferation regulating genes in hNPCs, we performed four separate CRISPR-Cas9 screens to identify genes which, when knocked out, cause increased expansion of hNPCs. We used three separate CRISPR-Cas9 libraries, two different time points (10 days versus ~3 weeks), and two different human NPC isolates, CB660 and U5 (Bressan, Dewari et al., 2017, Pollard et al., 2006, Toledo, Ding et al., 2015) (Figs 1A-C and S1A, Table S1).

These screens revealed dozens of candidate antiproliferative screen hits, which were enriched for known tumor suppressor genes (Futreal, Coin et al., 2004) (Fig S1B) and genes found mutated across 35 different cancer types (Fig 1D). In contrast to NPCs, there was little evidence of expansion enhancement in CRISPR-Cas9 screens for patient-derived glioblastoma stem cell-like (GSCs) isolates (Joo, Kim et al., 2013) grown in the same conditions (Fig S1C), consistent with pre-existing, cancer-associated disruptions of key proliferative and tumor suppression pathways.

Examining the intersection of all of our screen data revealed five reproducible and robust proliferation-enhancing screen hits: *CREBBP*, *NF2*, *PTPN14*, *TAOK1*, and *TP53* (Fig 1E), which we validate, examine, and discuss below.

Validation of *CREBBP*, *NF2*, *PTPN14*, *TAOK1*, and *TP53 as* antiproliferative genes in hNPCs

To control for off-target effects, we performed small guide RNA (sgRNA) tiling screens for each of these genes, whereby each gene is targeted with 138 to 466 sgRNAs tiled across most exons. At least 70% of tiling sgRNAs for each candidate

proliferation limiting gene were significantly enriched in NPCs, whereas an sgRNA tiled gene essential for DNA replication, *MCM2*, showed significant depletion over time and control, non-targeting (NTC) sgRNAs were largely inert (Figs 2A and S2A; Table S1). KO of target genes was confirmed by Western blots (Fig 2B) and by deep sequencing analysis for *CREBBP*, *NF2*, and *TP53* (Toledo et al., 2015).

KO of *CREBBP, NF2, PTPN14, TAOK1,* and *TP53* in hNPCs caused a significant proliferative advantage over control cells in a 23-day outgrowth competition assay, while KO of the essential gene *KIF11* showed the opposite result (Fig 2C). However, the competitive advantage did not appear to be based on differences in survival since no changes in Annexin-V staining were observed following normal culturing or in co-cultures, where apoptosis remained <2% regardless of the experimental condition.

Using cell proliferation assays (Fig 2D-G), we found that each KO significantly increased cell accumulation in 48-96 hour outgrowth assays. Importantly, this effect was independent of cell density, as KO cells showed increased proliferation at both low and high densities (e.g., Fig 2E,F). Further, the doubling time significantly decreased for each KO, shortening from ~50 hours to 30-40 hours (Fig 2H), similar to two GSC isolates used in the same assay.

A transient G0-like state is skipped in NPCs after KO of *CREBBP*, *NF2*, *PTPN14*, *TAOK1*, or *TP53*

In order to further investigate changes in cell cycle dynamics, we utilized the fluorescent ubiquitination cell cycle indicator (FUCCI) system (Sakaue-Sawano,

Kurokawa et al., 2008). Figure 3A shows typical results from control experiments in U5-NPCs, where ~63% of cells are in G0/G1, ~15% are in S/G2/M, while the remainder are transitioning between these phases. KO of *CREBBP*, *NF2*, *PTPN14*, *TAOK1*, or *TP53* caused dramatic loss of the G0/G1 population (reducing the frequency to 47-38%) and significantly lowered the ratio of G0/G1 to S/G2/M cells (~2-4 fold lower) (Fig 3B,C).

We also measured transit time through G0/G1 and S/G2/M in individual NPCs using time-lapse microscopy (Fig S2B-E). For G0/G1 transit times, we found that our control hNPCs exhibit variable G1 transit times, consistent with observations of a transient G0-state seen in other non-transformed human and rodent cells (Spencer, Cappell et al., 2013). We observed a wide distribution of G0/G1 transit times in control hNPCs, from fast (4.3 hrs), medium, and extremely slow (95 hrs) (averaging 32.5 hrs) (Fig 3d). By contrast, S/G2/M transit times were much more uniform (~12.4 hrs).

KO of *CREBBP*, *NF2*, *PTPN14*, *TAOK1*, or *TP53* dramatically collapsed the distributed G0/G1 transit times leading to a highly significant, faster transit of <11.7 hrs in KOs ($p<0.0001$) (Fig 3D). However, S/G2/M transit times were not significantly affected. Intriguingly, GSCs also exhibit collapsed and faster G0/G1 transit times (Fig 3D).

To further examine possible changes in G0/G1 dynamics, we examined molecular features associated with G0, G1, and late G1 (Fig 4A), including Rb phosphorylation, CDK2 activity, and p27 accumulation.

In mammals, cell cycle ingress is governed by progressive phosphorylation of Rb by CDK4/6 and CDK2 as cells pass through the restriction point in late G1, causing de-repression of E2F transcription factors (Sherr & McCormick, 2002, Weinberg, 1995,

Yao, Lee et al., 2008, Zetterberg, Larsson et al., 1995). We observed that KO of *CREBBP*, *NF2*, *PTPN14*, *TAOK1*, or *TP53* in U5-NPCs results in a pronounced increase in the intensity of phosphorylated Rb during G1, consistent with an enrichment for a late G1 state (Fig 4B).

CDK2 activity correlates with cell cycle progression; if CDK2 activity levels are low during G1, cells enter G0 (Spencer et al., 2013). If CDK2 activity is intermediate (relative to its peak during G2/M) they progress past the restriction point and into S-phase (Spencer et al., 2013). Using the steady-state cytoplasmic to nuclear ratios of a DNA helicase B (DHB)-mVenus reporter as a readout of CDK2 activity (Hahn, Jones et al., 2009, Spencer et al., 2013), we observed significant increases in CDK2 activity in each KO in G0/G1 cells (Fig 4C,D). This was true either by total intensity or the proportion of cells with a reporter ratio greater than 1, which corresponds with S-phase entry in mammary epithelium (Spencer et al., 2013). Control cells averaged ~8% of G1 cells with >1 cytoplasmic:nuclear reporter ratios CDK2 activity, while KOs were 20-27% (Fig 4D).

Another hallmark of G0/quiescence is the stabilization of p27, a G1 cyclin-dependent kinase (CDK) inhibitor required for maintaining G0 (Coats, Flanagan et al., 1996, Susaki, Nakayama et al., 2007). Consistent with loss of transient G0 cells, we observed that KO of *CREBBP*, *NF2*, *PTPN14*, *TAOK1*, or *TP53* resulted in significant reduction of p27 levels in proliferating NPCs (Fig 4E,F).

Collectively, the above data demonstrate that KO of antiproliferative genes in U5-NPCs causes a cell autonomous decrease in cell cycle length with less distributed and faster G0/G1 transit times, an increase in the molecular features associated with late

G1, and a reduction in the molecular features associated with G0 (Fig 4G). These data are consistent with KOs either blocking entry of cells into a transient G0 state or causing failure to maintain cells in G0. Therefore, we call these G0-skip genes.

G0-skip genes have overlapping but distinct roles in regulating G0/G1 gene expression

To further characterize G0-skip genes, we performed gene expression analysis of KO cells specifically in G0/G1 phase. Among our G0-skip genes, it has been previously reported that *TP53*/p53 and its transcriptional target *CDKN1A*/p21 have causal roles in modulating entry into G0 (Arora, Moser et al., 2017, Barr, Cooper et al., 2017, Spencer et al., 2013, Yang, Chung et al., 2017). Consistent with this notion, *CDKN1A* KO scored as a proliferation enhancer of U5-NPCs using the 3rd generation CRISPR-Cas9 library (Fig S1A). Thus, one key question is whether each of the other G0-skip genes merely acts through p53 and/or p21 to regulate G0. CREBBP/CBP, for example, has been implicated in positively regulating p53 turnover and activity via acetylation (Ito, Lai et al., 2001).

Other G0-skip genes have known or suspected roles in negatively regulating Hippo-YAP pathway signaling which regulates cell and tissue growth and response to contact inhibition (Yu, Zhao et al., 2015). For the latter, repression of Hippo signaling is sufficient to arrest cells in G0/G1 at high densities (Zhao, Wei et al., 2007); however, our phenotypes occur at sub-confluent densities, suggesting that precocious Hippo-YAP activation rather than bypass of contact inhibition would be driving Hippo-YAP-related effects. NF2 (Neurofibromin 2, Merlin), PTPN14, and TAOK1 have been demonstrated

or proposed to negatively regulate YAP, the major downstream effector of HIPPO signaling, through modulating LATS1/2 kinase activity (Plouffe, Meng et al., 2016, Wilson, Li et al., 2014, Zhang, Bai et al., 2010) or, in the case of PTPN14, through preventing nuclear localization of YAP (Lin, Poon et al., 2013).

To analyze gene expression, RNA-seq was performed on mCherry-CDT1+ sorted NPCs after KO, which captures both G0 and G1 subpopulations (Fig 5A and Table S2). In control NPCs, as expected, comparing G0/G1 sorted cells to unsorted populations revealed down-regulation of genes involved in cell cycle regulation, DNA replication, and mitosis (Fig 5A and Table S3). Overall comparisons between the KOs and NTC U5-NPCs showed that KO of *NF2* and *PTPN14* were most similar by unsupervised clustering as well as having the most overall gene changes, while *TAOK1* KO was most similar to the controls (Fig 5B). However, comparison of the overlapping up- or down-regulated genes showed that *TAOK1* KO up-regulated genes were more similar to *NF2* and *PTPN14* KO than the other KOs (Fig S3A).

First evaluating p53 target genes, we found that only *TP53* KO significantly down-regulated the expression of high confidence p53 targets including *BAX*, *CDKN1A/p21, RRM2B,* and *ZMAT3* (Fischer, 2017) (Figs 5C and S3B). None of the other KOs showed inhibition of p53 targets or p53 itself, strongly suggesting that the G0-skip genes are not acting through p53-dependent transcriptional activity.

For evaluation of the transcriptional targets of the HIPPO-YAP pathway, we examined the expression of 55 YAP conserved gene targets (Cordenonsi, Zanconato et al., 2011). Each KO, except for *CREBBP*, showed significant enrichment for YAP targets with *NF2* KO having increased expression of the largest subset (Figs 5C and

S3C). Interestingly, *NF2* KO activated one subset of YAP targets important in the biological process of extracellular matrix (ECM) organization, while *TAOK1* KO activated a different subset of YAP targets important in nuclear chromosome segregation, such as during mitosis (Fig S3C-E). *NF2* and *PTPN14* KO shared the most overlap in YAP target activation, including targets considered universal Hippo-YAP targets (e.g., *CTGF*, *CYR61*, and *SERPINE1*).

Examining changes in other cell cycle regulatory genes (Figs 5C and S3F) revealed that G1 cyclins, *CCND1* and *CCND2* were up-regulated to varying degrees in all KOs, except for *TAOK1*. In turn, *TAOK1* KO causes inappropriate up-regulation of *CCNA2* (which has been shown to cause premature S-phase entry from G0 and G1 when overproduced) (Resnitzky, Hengst et al., 1995), *CCNB1*/*2*, and other mitotic genes. Moreover, expression of *MYC*, which is vitally important for NPC proliferation (Wey, Martinez Cerdeno et al., 2010), was also increased following *NF2*, *PTPN14*, and *TP53* KO. *CREBBP* KO cells up-regulated *HRAS*, which can trigger exit from quiescence(Feramisco, Gross et al., 1984), and dramatically down-regulated *CDKN1C*/p57/KIP2 (>8-fold), a key G1 CDK inhibitor required for NSC quiescence during adult neurogenesis (Furutachi, Matsumoto et al., 2013) and *CDKN1B*/p27. *PTPN14* and *TP53* KO also down-regulated *CDKN1C*, although only 2 to 3-fold.

We next performed gene ontology (GO) analysis for genes up- or down-regulated after KO (The Gene Ontology, 2017) (Figs 5D,E and S4A,B; Supplementary Table 4). For up-regulated genes, the only common biological processes related to extracellular matrix and structure organization. Among up-regulated gene sets, *NF2* and *PTPN14* KO again showed the most overlap with 127 GO categories, while up-regulation of various

Hippo-YAP pathway members, including *LATS2*, *TEAD1,* and *YAP1*, suggests a possible feedback regulation of the pathway unique to *NF2* and *PTPN14* KO (Fig S4C).

There were also a number of notable categories unique to some KOs among up-regulated genes. Intriguingly, *TAOK1* KO triggered up-regulation of >40 key regulators of mitosis (e.g., *AURKA*, *BUB1*, *CCNB1/2*, *CDK1*, *KIF11*, *etc.*), suggesting it may act to inhibit their precocious activation in G0/G1 or expression after mitosis has completed (Fig S4D). *CREBBP* KO caused up-regulation of key nuclear-encoded mitochondrial genes, including members of the NADH dehydrogenase complex, the succinate dehydrogenase complex, and mitochondrial DNA polymerase (Fig S4E). Since many of these genes are direct transcriptional regulatory targets of nuclear respiratory factors 1 and 2 (NRF1 and NRF2) (Kelly & Scarpulla, 2004), CREBBP likely acts to oppose NRF1/2 function in G0/G1 and to attenuate cellular respiration and mitochondrial function.

Analysis of down-regulated gene sets shared among all KOs revealed significant enrichment for genes involved in neural development with categories such as nervous system development, regulation of neurogenesis, and glial cell differentiation (Figs 5E and S4B). In addition, many other components of neural differentiation are down-regulated among subsets of the G0-skip genes, including regulation of synaptic plasticity, membrane potential, oligodendrocyte differentiation, and dendrite development, suggesting that G0-skip genes help maintain neurodevelopmental gene expression in G0/G1.

Identification of candidate G0 and G1 subpopulations in NPCs impacted by G0-skip mutants

To identify a transcriptional profile for G0 NPCs, we performed single-cell RNA sequencing (scRNA-seq) on both unsorted NPCs and G0/G1 sorted cells. ScRNA-seq has recently been used to resolve heterogeneous populations of cells as well as cell cycle phases (Macosko, Basu et al., 2015, Zheng, Terry et al., 2017). To this end, we analyzed the results from 5973 unsorted and 4562 mCherry-hCDT1 sorted hNPCs (Methods). For the unsorted populations, we then performed unbiased cluster analysis and identified seven prominent clusters each defined by a set of transcriptionally enriched and depleted genes (Figs 6A and S5A, and Table S4). We categorized the clusters by examining: cell cycle gene expression hallmarks, gene set enrichment, cluster network analysis, scRNA-seq from G0/G1 sorted populations, and scRNA-seq data sets examining adult rodent neurogenesis (Fig 6). We defined the clusters in normal, cultured hNPCs as follows: Neural G0 (17.3% of cells), G1 (36.7%), Late G1 (6.4%), S (7.2%), S/G2 (10.9%), G2/M (10.6%), and M/early G1 (8.4%) (Fig 6b).

The S, S/G2, and G2/M clusters were enriched for genes whose expression peaks in these phases (Cyclebase (Santos, Wernersson et al., 2015)) including *CCNE2* in S-phase and *CCNB1/2* in G2/M (Figs 6C and S5C) and produced tightly interconnected networks of key cell cycle genes (Fig S5D). This enrichment included the DNA replication genes *PCNA, MCM3/4/5/6/7/10, GMNN, and RPA2/3* for S-phase and the mitosis genes *CDC20*, *AURKA*, and *BUB1* during G2/M.

There were four definable G0/G1 clusters (Figs 6B and S5B). Despite being the largest cluster, the G1 cluster had the smallest number of enriched identifying genes

which included IGFR1 signaling genes (e.g., *IGFBP3* and *IGFBP5*), and significant reductions of genes expressed in S, S/G2, and G2/M clusters (Fig S5C). The M/early G1 cluster showed low but significant residual expression of M phase genes and enrichment for splicing factor genes. The Late G1 cluster was defined by genes important in G1 cell cycle progression, including *CCND1* and *MYC*, and enriched for cholesterol biosynthesis, cell adhesion genes, and the subset of YAP target genes activated following *NF2*/*PTPN14* KO, such as *CTGF* and *SERPINE1* (Figs 6C and S6A).

Finally, the Neural G0 cluster also showed significant repression of genes peaking in other phases of cell cycle, including suppression of *CCND1* expression, which is an indicator of cell cycle exit (Sherr, 1995). Moreover, this population uniquely showed significant enrichment for many types of neural development gene categories, including glial cell differentiation, neurogenesis, neuron differentiation, and oligodendrocyte differentiation (Table S5). These genes included transcription factors with known roles in balancing stem cell identity and differentiation, including *OLIG2*, *HEY1*, *HOPX*, *BEX1*, *SOX2, SOX4*, and *SOX9* (Bergsland, Werme et al., 2006, Sakamoto, Hirata et al., 2003, Scott, Wynn et al., 2010).

Network analysis of mean and overlapping cluster gene expression resolved the seven clusters into a pattern that fits well with cell cycle progression and predicted transit through G0/G1 (Fig 6D). The gene expression of the candidate G0 population only significantly overlapped with G1 cluster, consistent with a cell cycle exit from G1.

Comparison of our scRNA-seq cell clusters to gene expression profiles derived from *in vivo* neurogenesis samples supported our definition of this cluster as G0. In two

independent scRNA-seq analyses of rodent neurogenesis (Artegiani, Lyubimova et al., 2017, Llorens-Bobadilla, Zhao et al., 2015), the Neural G0 cluster showed most significant enrichment for genes defining quiescent neural stem cells and oligodendrocyte precursors (Fig S6D). These genes include, among others: *CLU*, *HOPX*, *ID3*, *OLIG2, PTN*, *SYT11*, *S100B*, *SOX9*, *PTPRZ1*, and *TTYH1* (Fig 6e,f). Interestingly, for our S, S/G2, G2/M, and M/early G1 cluster genes, we found significant overlap with the activated NSCs of Llorens-Bobadilla et al. (2015) and the NPCs of Artegiani et al. (2017) (Fig S6D), which are no longer quiescent.

Lastly, we applied our cluster criteria to a scRNA-seq dataset from mouse embryonic stem cells (mESCs) sorted by live Hoechst staining into G1, S-phase, and G2/M populations (Buettner, Natarajan et al., 2015). We found that our G1 category captured 83% of their Hoechst G1 cells, our G2/M category captured 89% of their G2/M, and their S-phase cells were split between G1, S, and G2/M, which is consistent with their Hoechst S-phase gate overlapping portions of these populations (Fig S6C). However, the mESCs failed to score in our Neural G0, Late G1, or M/early G1 categories. This is consistent with the shorter G1 of ESCs compared to somatic cells (Coronado, Godet et al., 2013) and suggests that these G0/G1 subpopulations may be unique to adult or tissue-specific stem cells.

These results demonstrate that hNPCs have definable G0 and G1 subpopulations and that the candidate G0 population is uniquely enriched for expression of neurodevelopment genes, including those associated with quiescent NSCs.

KO of G0-skip genes results in transcriptional reprogramming of genes associated with G0/G1 NPC subpopulations

We next examined if genes defining each of the scRNA-defined clusters were significantly changed in the RNA-seq profiles of KO NPCs (Fig 7A,B). The analysis revealed that genes associated with the Neural G0 cluster were significantly down-regulated after KO of *CREBBP*, *NF2*, *PTPN14*, *TAOK1*, or *TP53*. These genes included those expressed in quiescent NSCs and others cited above with key roles in neural development (e.g., *CLU*, *HOPX*, *ID3*, *PTN*, *PTPRZ1*, *SOX2*, and *SOX4*) (Fig S7A).

By contrast, we found that genes associated with the late G1 cluster, including *CCND1* and *MYC*, are significantly up-regulated in each KO (Fig S7B). Further, we find KO *TAOK1*, and to a lesser degree, *PTPN14*, caused up-regulation of S/G2, G2/M, and M/early G1 associated genes.

To further confirm these results, scRNA-seq was performed on G0/G1-sorted hNPCs with KO of *TAOK1*, since its KO produced the largest degree of cross-cluster G0/G1 gene expression changes (Fig 7A). The Neural G0 population and, to a lesser degree, G1 in *TAOK1* KO cells is significantly diminished from 21.3% to 10.3% and 58.9% to 53.3%, respectively (Fig 7C-E). However, the late G1 population is increased (from 3.0% to 9.8%) as are cells in the M/early G1 (from 7.8% to 15.3%) and G2/M phase (from 1.5% to 4.4%). The expansion of the M/early G1 in *TAOK1* KO cells explains and cross-validates the increase in mitotic genes observed in the bulk G0/G1 RNA-seq data in *TAOK1* KO cells (Fig S4D), suggesting that TAOK1 helps attenuate expression of mitotic genes from the previous cell cycle.

These results strongly suggest that G0-skip mutants lose a significant fraction of the hNPC Neural G0 subpopulation and reprogram G1 transcription networks to promote entry into G1-S. We also examined the G0/G1 gene expression profiles from two patient GSC isolates to see if we could identify changes in similar G0/G1 cell cycle subpopulations in cancer cells (Fig S7C,D and Table S2). We found that genes associated with G1 or Neural G0 were depleted in the sorted GSCs, consistent with the decreased G0/G1 transit time seen through time-lapse FUCCI analysis (Fig 3D). There was a greater increase in genes related to S and S/G2 in G0/G1 than in the NPCs and limited changes in genes associated with Late G1, suggesting that there may be other G1 subpopulations altered in the GSCs.

Loss of G0-skip genes attenuates developmental programs during hNPC differentiation

Since G0-skip mutants affect subpopulations of NPCs enriched for expression of neural genes, we further examined if KO of G0-skip genes affects developmental transcriptional programs triggered upon hNPC differentiation. To this end, we differentiated hNPCs by removal of mitogenic growth factors, FGF2 and EGF. These conditions trigger specification of multiple neural cell types over the course of 8 weeks, including TUJ1+ neurons, GFAP+ astrocytes, and a small number of O4+ oligodendrocytes. After only 7 days of mitogen-withdrawal, U5-NPCs show increased markers of the astrocytic and neuronal lineage (GFAP and TUJ1, respectively) and radial glia markers (*GFAP*, *VIM*, *GLI3*, *PAX6*, *SOX2*), reduction of neural stemness-related genes (e.g., *NES*/Nestin, *PROM1*/CD133), and an elongated, bipolar

morphology (Fig S7E and Table S6). There are also increases in 93 brain-specific/restricted transcription factors (e.g., *BCL11B*/CTIP2, *NEUROD1*, *POU3F2*/BRN2, *RFX4*, *ZBTB18*, *ZIC4*, etc.) (Gray, Fu et al., 2004) (Table S6) and genes associated with cell-cell adhesion, extracellular matrix organization, synapse assembly, and axoneme assembly. Consistent with exit from the cell cycle during this differentiation, we find genes involved in mitosis, DNA replication, and G1/S transition are significantly reduced (Table S6).

Among G0-skip genes, *NF2* and *PTPN14* KO more closely resembled each other and undifferentiated cells (Supplementary Fig 7f). Further, their KO also prevented up-regulation of most of the 93 neural transcription factors (59 total) up-regulated during early differentiation, while other KOs overlapped these 59 to varying degrees (Fig S7G). These included GATA2, which drives NPCs out of the cell cycle concomitant with down-regulation of cyclin D1 expression and up-regulation of p27/Kip1 (El Wakil, Francius et al., 2006), and FOXJ1, which controls NPC fate determination (Li, Floriddia et al., 2018). Moreover, we found that G0-skip mutants disrupt the early neural differentiation transcriptional programs, including reduced *GFAP* expression, reduced cilia-related genes (including *DRC1*), and reduced synapse-assembly genes (Figs 7F and S7H).

CREBBP and *PTPN14* KO cells were more mitogen-independent, maintaining enrichment for cell cycle genes even after the withdrawal of FGF2 and EGF to induce differentiation (Table S7 and Fig 7G). In contrast, *TP53* KO cells showed the most mitogen-dependence, with almost all cell cycle genes examined down-regulated similar to and even beyond values in control cells. *NF2* KO cells displayed a partial effect with

Late G1/S genes up-regulated (e.g., *CCND1*, *CCNE1*, and *MYC*), but no observable enrichment for key mitotic genes.

Thus, KO of G0-skip genes affect neurodevelopmental gene expression during conditions favoring lineage commitment, suggesting that the Neural G0 subpopulation may play an important role in maintaining fidelity of neurodevelopmental transcription programs.

DISCUSSION

Here we report the identification and characterization of five genes, *CREBBP*, *NF2*, *PTPN14*, *TAOK1*, and *TP53*, that function in hNPCs to limit proliferation through the promotion of a definable G0-like state (Fig 7H). KO of these genes causes decreased hNPC doubling time by triggering less distributed and faster G0/G1 transit times (Figs 2 and 3), while reducing molecular features associated with G0 in G1 subpopulations (Figs 4, 5, and 7). Our results are consistent with the notion that these G0-skip mutants cause significant loss of a G0-like population, which we have named Neural G0, since it is highly enriched for expression of genes associated with quiescent NSCs and neurodevelopment.

Our results provide key biological insights into a recently proposed model of cell cycle exit. In mammals, cell cycle ingress is governed by the restriction point, a bistable transcriptional switch that converts growth stimuli into all-or-none E2F transcriptional responses and irreversibly commits cells into the cell cycle (Sherr & McCormick, 2002). However, a second restriction point was recently proposed for cell cycle exit, which is governed by the amount of residual CDK2 activity from the previous cell cycle (Spencer

et al., 2013). In mammalian cell lines, this restriction point is modulated by the presence of endogenous DNA damage and mitogen-driven Ras signaling during the previous cell cycle, which determine entry into a transient G0-like state in the next cell cycle (Arora et al., 2017, Barr et al., 2017, Naetar, Soundarapandian et al., 2014, Yang et al., 2017). Critical molecular determinants include p53-dependent *CDKN1A/*p21 expression and mitogen-dependent modulation of Cyclin D mRNA levels in G2/M and G0/G1 (Yang et al., 2017).

Consistent with this second restriction point operating in cultured hNPCs, we observe a variable length G0/G1 with a portion of hNPCs entering a transient G0-like state each cell cycle. We further demonstrate that *TP53*, which regulates *CDKN1A/p21* expression in hNPCs, is required for this transient G0-arrest. Moreover, we identify p53-independent effectors that likely act through Hippo-YAP signaling pathway (*NF2* and *PTPN14*) or via novel mechanisms (e.g., *CREBBP* and *TAOK1*) to affect expression of genes that allow bypass or escape of the G0-like state (e.g., *MYC*, *HRAS*, *CCND1/2*, *CCNA2*, *CDKN1B*/p27) (Figs 5C and S3).

Further, using scRNA-seq, network, and molecular analysis, we defined the gene expression signature associated with this G0-like state. This signature prominently featured neurodevelopmental genes and genes specifically expressed in quiescent NSCs in post-natal mice (Fig 6F), which were not found significantly expressed in other hNPC cell cycle populations. Since *CREBBP*, *NF2*, *PTPN14*, *TAOK1*, and *TP53* KO both decrease residence in a G0-like state and disrupt differentiation specification, the results are consistent with Neural G0 being important for hNPC development potential, at least *in vitro* (Figs 7F,G and S7E-H).

Changes in the length of G1 can affect cell-fate specification. During cerebral development, fast dividing multipotent stem/progenitor cells that first populate the neocortex have a short G1, and, as lineage-commitment occurs, neuro-progenitors' cell cycle is slowed by lengthening G1 phase, eventually giving rise to post-mitotic, terminally differentiated cells (Miyama, Takahashi et al., 1997, Takahashi, Nowakowski et al., 1995). Experimentally modulating G1 length of cortical progenitors *in vivo* via up or down-regulating Cyclin D-Cdk4 activity can inhibit or enhance neurogenesis of cortical progenitors(Lange, Huttner et al., 2009). Thus, lengthening of G1, i.e., transient cell cycle exit, has been proposed to help reinforce priming and maintenance of lineage-specific development programs (Calegari & Huttner, 2003, Lange et al., 2009, Singh, Chappell et al., 2014).

The G0-skip genes also may affect the proliferation and self-renewal balance *in vivo.* Neurogenesis studies in rodents have documented preferential p53 protein expression, low-level p53 transcriptional activation, including p21 activation, and negative regulation of neural stem/progenitor cell proliferation in neurogenic regions of embryonic and postnatal brains (Gil-Perotin, Marin-Husstege et al., 2006, Gottlieb, Haffner et al., 1997, Komarova, Chernov et al., 1997, Meletis, Wirta et al., 2006, van Lookeren Campagne & Gill, 1998). Further, *Nf2* has been shown to prevent overexpansion of neural progenitors during mouse neurogenesis (Lavado, He et al., 2013).

Lastly, our results also suggest that G0-skipping could play unexpected roles in developing neoplasms, as the G0-skip genes are among the most highly mutated across 35 different tumor types (Fig 1D). In addition to faster proliferation, if the

transient G0-like state has dual roles in maintaining developmental potential and allowing time to repair DNA damage, then G0-skipping could simultaneously reduce the barrier to adopt alternative developmental states and promote genomic instability. In glioblastoma patient isolates, we observe phenotypes consistent with G0-skipping, including uniform, fast G1 transit times and diminished Neural G0 gene expression in G0/G1 populations (Figs 3D and S7B).

Collectively, this work reveals novel aspects of the proliferation of cultured hNPC through the use of functional genetics and single- and subpopulation-resolved genomic profiling, which may further aid in understanding NPC biology. These data are also a novel resource for the study of *CREBBP*, *NF2*, *PTPN14*, *TAOK1*, and *TP53* and the dynamics of stem cell proliferation, including a detailed transcriptional model of the hNPC cell cycle.

Materials and Methods

Cell culture

NPC and GSC lines were grown in NeuroCult NS-A basal medium (StemCell Technologies) supplemented with B27 (Thermo Fisher Scientific), N2 (2x stock in Advanced DMEM/F-12 (Thermo Fisher) with 25 μg/mL insulin, 100 μg/mL apo-Transferrin, 6 ng/mL progesterone, 16 μg/mL putrescine, 30 nM sodium selenite, and 50 μg/mL bovine serum albumin (Sigma), and EGF and FGF-2 (20ng/mL each) (Peprotech) on laminin (Sigma or Trevigen) coated polystyrene plates and passaged according to previously published protocols (Pollard, Yoshikawa et al., 2009). Cells

were detached from their plates using Accutase (EMD Millipore). 293T (ATCC) cells were grown in 10% FBS/DMEM (Thermo Fisher).

Lentiviral production

For virus production, lentiCRISPR v2 plasmids (Sanjana et al., 2014) were transfected using polyethylenimine (Polysciences) into 293T cells along with psPAX and pMD2.G packaging plasmids (Addgene). To produce lentivirus for the whole-genome CRISPR-Cas9 libraries, 25x150mm plates of 293T cells were seeded at ~15 million cells per plate. Fresh media was added 24 hours later and viral supernatant harvested 24 and 48 hours after that. For screening, virus was concentrated 1000x following ultracentrifugation at 6800*xg* for 20 hours. For validation, lentivirus was used unconcentrated at an MOI<1.

CRISPR-Cas9 screening

For large-scale transduction, NPC cells were plated into T225 flasks at an appropriate density such that each replicate had 250-500-fold representation, using the two previously published CRISPR-Cas9 libraries (Doench, Fusi et al., 2016, Shalem, Sanjana et al., 2014) (Addgene) or a custom synthesized sgRNA library (Twist Biosciences) targeting 1377 genes derived from (Toledo et al., 2015). Full lists of the guides are in Table S3. NPCs and GSCs were infected at MOI <1 for all cell lines. Cells were infected for 48 hours followed by selection with 1-2 μg/mL (depending on the target cell type) of puromycin for 3 days. Post-selection, a portion of cells were harvested as Day 0 time point. The remaining cells were then passaged in T225 flasks

maintaining 250-500-fold representation and cultured for an additional 21-23 days (~10-15 cell doublings) or 10 days. Genomic DNA was extracted using QiaAmp Blood Purification Mini or Midi kit (Qiagen).

A two-step PCR procedure was performed to amplify sgRNA sequence. For the first PCR, DNA was extracted from the number of cells equivalent to 250-500-fold representation (screen-dependent) for each replicate (2-4 replicates) and the entire sample was amplified for the guide region. For each sample, ~100 separate PCR reactions (library and representation dependent) were performed with 1 µg genomic DNA in each reaction using Herculase II Fusion DNA Polymerase (Agilent) or Phusion High-Fidelity DNA Polymerase (Thermo Fisher). Afterwards, a set of second PCRs was performed to add on Illumina adaptors and to barcode samples, using 10-20ul of the product from the first PCR. Primer sequences are in Table S8. We used a primer set to include both a variable 1-6 bp sequence to increase library complexity and 6 bp Illumina barcodes for multiplexing of different biological samples. The whole amplification was carried out with 12 cycles for the first PCR and 18 cycles for the second PCR to maintain linear amplification. Resulting amplicons from the second PCR were column purified using Monarch PCR & DNA Cleanup Kit (New England Biolabs; NEB) to remove genomic DNA and first round PCR product. Primers sequences are available in Table S8. Purified products were quantified (Qubit 2.0 Fluorometer; Fisher), mixed, and sequenced using HiSeq 2500 (Illumina).

Bowtie was used to align the sequenced reads to the guides (Langmead, Trapnell et al., 2009). The R/Bioconductor package edgeR was used to assess changes across various groups (Robinson, McCarthy et al., 2010). For the tiling library, only

guides that mapped once to the genome and are within the gene's coding region were considered for further analysis. Raw and mapped data files are available at the Gene Expression Omnibus database (GSE117004).

Individual lentiviral-sgRNA assembly for validation

For retests, individual or pooled sgRNA were cloned into lentiCRISPR v2 plasmid. Briefly, DNA oligonucleotides were synthesized with sgRNA sequence flanked by the following:

5': tatatcttGTGGAAAGGACGAAACACCg

3': gttttagagctaGAAAtagcaagttaa

PCR was then performed with the ArrayF and ArrayR primers (Table S8). The PCR product was gel purified using the ZymoClean Gel DNA recovery kit (Zymo Research). Gibson Assembly Master Mix (NEB) was used to clone the PCR product into lentiCRISPR v2 plasmid (Sanjana, Shalem et al., 2014). The ligated plasmid was then transformed into Stellar Competent cells (Clontech), and streaked onto LB agar plates. The resulting clones were grown up and sequence verified (GeneWiz).

Viability and Proliferation Assays

Cells were infected with lentiviral gene pools containing 3-4 sgRNAs per gene or with lentivirus containing a single sgRNA to the respective gene (Table S8). Initial cell density was carefully controlled for in each experiment by counting cells using a Nucleocounter NC-100 (Eppendorf) and cells were always grown in subconfluent conditions. For viability assays, following selection, cells were outgrown for 7-10 days,

then harvested, counted, and plated in triplicate onto 96-well plates coated with laminin in dilution format starting at 1,000 cells to 3,750 cells per well (cell density depended on cell isolate and duration of assay). Cells were fed with fresh medium every 3-4 days. After 7-12 days under standard growth conditions, cell proliferative rates were measured using Alamar blue reagent according to manufacturer's instructions (Invitrogen). For analysis, sgRNA-containing samples were normalized to their respective nontargeting control (NTC) samples. For doubling time assays, cells infected with individual sgRNAs or NTC were routinely cultured (split every 3-5 days), and counted at each split (Nucleocounter NC-100; Eppendorf). The overall growth of each well containing an individual sgRNA was calculated and compared to the NTC well. Comparisons between multiple experiments were normalized.

Competition experiment

NPCs were infected with lentiviral gene pools containing 3-4 sgRNAs per gene, puromycin selected, and mixed with NPCs infected with lentiviruses containing turboGFP at an approximate 1:9 ratio, respectively. Cultures were outgrown for 23 to 31 days and flow analysis (FACS Canto; Becton Dickinson) was conducted every 7-8 days for GFP expression. Flow analysis data was analyzed using FlowJo software. For each sample, the GFP- population for each time point was normalized to its respective Day 0 GFP- population and the NTC (competition index).

Time-lapse microscopy

NPCs were infected with lentiviral gene pools containing 3-4 sgRNAs per gene or with individual sgRNAs, puromycin selected, outgrown for >13 days, and plated onto 96-well plates or 24-well plates. Plates were then inserted into the IncuCyte ZOOM (Essen BioScience), which was in an incubator set to normal culture conditions (37° and 5% CO_2), and analyzed with its software. For the cell confluency experiment, phase images were taken every hour for 72 hours. For the FUCCI cell cycle experiment, images were taken every 10-15 minutes for 72-120 hours. Cell cycle transit time for G0/G1 (mCherry-CDT1(aa30-120)+) and S/G2/M (mAG-Geminin(aa1-110)+) was manually scored by three different observers in actively dividing cells (those that could be followed from mitosis to mitosis). Each KO was scored by at least 2 independent observers and consistency between scorers was checked through shared analysis of a standard.

Western blotting

Cells were harvested, washed with PBS, and either immediately lysed or snap-frozen and stored at -80˚C until lysis. Cells were lysed with modified RIPA buffer (150mM NaCl, 50mM Tris, pH 7.5, 2mM $MgCl_2$, 0.1% SDS, 2mM DDT, 0.4% deoxycholate, 0.4% Triton X-100, 1X complete protease inhibitor cocktail (complete Mini EDTA-free, Roche) and 1U/μL benzonase nuclease (Novagen) at room temperature for 15 minutes. Cell lysates were quantified using Pierce 660nm protein assay reagent and proteins were loaded onto SDS-PAGE for western blot. The Trans-Blot Turbo transfer system (Bio-Rad) was used according to the manufacturer's instructions. See Table S8 for antibodies and dilutions. An Odyssey infrared imaging system was used to visualize blots (LI-COR) following the manufacturer's instructions.

Flow Cytometry

FUCCI constructs (RIKEN, gift from Dr. Atsushi Miyawaki) were transduced into wild-type U5-NPCs and sorted sequentially for the presence of mCherry-CDT1(aa30-120) and S/G2/M mAG-Geminin(aa1-110) on an FACSAria II (BD). Normal growth was verified post-sorting and then the FUCCI U5-NPCs were transduced with individual sgRNA-Cas9 (4 independent guides per gene) and selected with 1 μg/mL puromycin. Cells were grown out for 21 days with splitting every 3-4 days and maintaining equivalent densities. Cells were counted (Nucleocounter NC-100; Eppendorf) and plated 3 days before analysis on an LSR II (BD). Controls cultured in the same conditions included cells transduced with guides against 3 non-growth limiting genes, including *GNAS1*, and showed equivalent FUCCI ratios. Results were analyzed using FlowJo software.

Immunofluorescence and CDK2 Activity

U5-NPCs were plated on acid-washed glass coverslips (phosphorylated Rb and CDK2 activity) or 96-well imaging plates (differentiation; Corning). They were fixed overnight in 2% paraformaldehyde (USB) at 4˚C, washed with DPBS (with calcium and magnesium) (Fisher), and blocked and permeabilized with 5% goat serum (Millipore), 1% bovine serum albumin (Sigma), and 0.1% triton X-100 (Fisher) in DPBS for 45 minutes at room temperature. Samples were stained with primary antibody diluted in 5% goat serum in DPBS overnight at 4˚C, washed with DPBS, and stained with secondary antibody (diluted 1:200 in 5% goat serum in DPBS) at 37˚C for 45 minutes. See Table S8 for antibodies and dilutions. Samples were washed with DPBS, dyed with 100 ng/mL 4',6-

diamidino-2-phenylindole (DAPI) diluted in DPBS for 20 minutes at room temperature, and washed with DPBS. Coverslips were preserved using ProLong Gold Antifade Mountant (Thermo Fisher) and inverted on glass slides. For differentiation, images were acquired on Nikon Eclipse Ti using NIS-Elements software (Nikon).

Phosphorylated Rb and CDK2 Activity Image Analysis

Cells were transduced with mVenus-DNA helicase B (DHB) (amino acids 994–1087) (Hahn et al., 2009) (gift from Dr. Sabrina Spencer) and the mCherry-*CDT1* FUCCI and sorted on a FACSAria II flow cytometer (BD). Cells were outgrown to ensure normal growth and then transduced with individual sgRNA-Cas9. After >10 days outgrowth, cells were counted and plated, grown for 2 days, and stained for phosphorylated Rb and imaged on a TISSUEFAXS microscope (TissueGnostics), 54 fields per KO or NTC. Cells were analyzed using CellProfiler (Kamentsky, Jones et al., 2011). G0/G1 nuclei were identified by the presence of the *CDT1* FUCCI reporter (25-120 pixel diameter, Global/Otsu thresholding, and distinguishing clumped objects by shape). CDK2 activity was defined by the cytoplasmic to nuclear ratio of the mVenus-DHB reporter, with the cytoplasmic intensity of the DHB reporter defined as the upper quartile intensity of a 2-pixel ring around the CDT1-defined nucleus due to the irregular shape of the U5-NPCs.

p27 reporter

The p27 reporter was constructed after (Oki et al., 2014), using a p27 allele that harbors two amino acid substitutions (F62A and F64A) that block binding to Cyclin/CDK complexes but do not interfere with its cell cycle-dependent proteolysis. This p27K^{-}allele

was fused to mVenus to create p27K^{-}-mVenus. To this end, the p27 allele and mVenus were synthesized as gBlocks (IDT) and cloned via Gibson assembly (NEB) into a modified pGIPz lentiviral expression vector (Open Biosystems). Lentivirally transduced cells were puromycin selected and validated using mCherry-CDT1 FUCCI and HDAC inhibitor treatment (48 hours of 5 μM apicidin (Cayman)) to induce G0/G1 arrest using FACS (LSR II from Becton Dickinson and FlowJo software).

Bulk RNA sequencing expression analysis

For G0/G1 NPC, cells singly positive for mCherry-*CDT1* FUCCI were sorted on a FACSAria II (BD) directly into TRIzol reagent (Life Technologies). For differentiating cells, cells were sparsely plated and cultured with growth medium without EGF or FGF-2 for 7 days before being lysed with TRIzol reagent. For both, 2 replicates per condition were harvested. RNA was extracted using Direct-zol RNA MiniPrep Plus (Zymo Research). Total RNA integrity was checked and quantified using a 2200 TapeStation (Agilent). RNA-seq libraries were prepared using the KAPA Stranded mRNA-seq Kit with mRNA capture beads (KAPA Biosystems) according to the manufacturer's guidelines. Library size distributions were validated using a 2200 TapeStation (Agilent). Additional library QC, blending of pooled indexed libraries, and cluster optimization was performed using the Qubit 2.0 Fluorometer (Thermo Fisher). RNA-seq libraries were pooled and sequencing was performed using an Illumina HiSeq 2500 in Rapid Run mode employing a paired-end, 50 base read length sequencing strategy.

Bulk RNA sequencing data analysis

RNA-seq reads were aligned to the UCSC mm10 assembly using Tophat2 (Trapnell, Roberts et al., 2012) and counted for gene associations against the UCSC genes database with HTSeq (Anders, Pyl et al., 2015). Differential expression analysis was performed using R/Bioconductor package edgeR (Robinson et al., 2010). Samples for G0/G1 bulk RNA-seq were collected in two batches, so batch-dependent genes were removed before analysis (inter-batch p-value<0.01 by Wilcoxon-Mann-Whitney). To ensure that no genes were eliminated that may be regulated specific to a particular knockout, genes with a CPM variability greater than 2-fold compared to the internal batch control and an expression greater than 1 CPM in at least one sample were retained. Differentially expressed genes (DEG) at the transcription level were found using a statistical cutoff of FDR < 0.05 and visualized using R/Bioconductor package pheatmap. Kolmogorov-Smirnov test were conducted in R using the function ks.test from stats package. Raw sequencing data and read count per gene data can be accessed at the NCBI Gene Expression Omnibus (GSE117004).

Gene ontology analysis

Gene Ontology (GO)-based enrichment tests were implemented using GOseq (v 1.23.0) (Young, Wakefield et al., 2010), which corrects for gene length bias. Gene lists were also analyzed for pathways using the R/Bioconductor package ReactomePA (v 1.15.4) (Yu & He, 2016). Analysis used all genes either up or down-regulated with a FDR<0.05 compared to NTC. GO terms with adjusted P-values<0.05 were considered significantly enriched. Venn diagrams were generated on http://bioinformatics.psb.ugent.be/webtools/Venn/.

Single cell RNA-sequencing Sample Preparation

Single cell RNA-sequencing was performed using 10x Genomics' reagents, instruments, and protocols. Single cell RNA-Seq libraries were prepared using GemCode Single Cell 3' Gel Bead and Library Kit. FUCCI U5-NPCs (both with and without lentiviral TAOK1 KO, >14 days outgrowth) were harvested and half the cells were sorted using the FACSAria II (BD) for cells singly positive for mCherry-CDT1 FUCCI. Sorted cells were kept on ice before suspensions were loaded on a GemCode Single Cell Instrument to generate single cell gel beads in emulsion (GEMs) (target recovery: 2500 cells). GEM-reverse transcription (RT) was performed in a C1000 Touch Thermal cycler (Bio-Rad) and after RT, GEMs were broken and the single strand cDNA cleaned up with DynaBeads (Fisher) and SPRIselect Reagent Kit (Beckman Coulter). cDNA was amplified, cleaned up and sheared to ~200bp using a Covaris M220 system. Indexed sequencing libraries were constructed using the reagents in the GemCode Single Cell 3' Library Kit, following these steps: 1) end repair and A-tailing; 2) adapter ligation; 3) post-ligation cleanup with SPRIselect; and 4) sample index PCR and cleanup. Library size distributions were validated for quality control using a 2200 TapeStation (Agilent). The barcoded sequencing libraries were quantified by a Qubit 2.0 Fluorometer (Thermo Fisher) and sequenced using HiSeq 2500 (Illumina) with the following read lengths: 98bp Read1, 14bp I7 Index, 8bp I5 Index and 10bp Read2. Sequencing data can be accessed at the NCBI Gene Expression Omnibus (GSE117004).

scRNA-seq Analysis

CellRanger (10x Genomics) was used to align, quantify, and provide basic quality control metrics for the scRNA-seq data. Using Seurat version 2.2.1, the scRNA-seq data from wild-type U5 cells and sgTAOK1 knock-out cells were merged and analyzed. Both scRNA-seq data were loaded as counts, normalized, and then scaled while taking into account both percent of mitochondria and the number of UMIs per cell as covariates. The union of the top 1,000 most variant genes from each dataset were used in canonical correlation analysis (CCA) to merge the two datasets via alignment of their subspace. We then identified clusters of cells using a shared nearest neighbor (SNN) modularity optimization-based clustering algorithm. Marker genes for each cluster were identified as differentially expressed genes, and the determination of 8 clusters was based on the discovery of strong markers for 6 of the eight clusters (both the G1 and low RNA clusters did not have significantly upregulated marker genes). Identity of clusters was determined primarily through the expression of cyclins and cyclin-dependent kinases, and secondarily through the function of other marker genes. A tSNE visualization was generated with a perplexity setting of 23.

Network analysis was used to determine the trajectories of cells through the cell cycle. First, the cluster centroids (mean expression for each gene across all the cells from a cluster) were used to compute the Canberra distance measure. In a cycle like a cell cycle, it is expected that on average there would be 2 edges between each cell cycle state. A distance cutoff of 240 led to 2.28 connections per cluster was used to turn the distance matrix into a network.

Network analysis of the clusters was performed using the STRING database (Szklarczyk, Morris et al., 2017) and visualized using Cytoscape software. Transcription factors were identified according to TFcheckpoint (Chawla, Tripathi et al., 2013).

Hypergeometric Analysis and Representation Factor Calculations

Hypergeometric tests (Johnson, Kemp et al., 2005) were carried out in R using function phyper (stat.ethz.ch/R-manual/R-devel/library/stats/html/Hypergeometric.html). Gene lists were prefiltered for the shared genes in each analysis to get the total gene population size, (i.e., 2739 genes for single cell analysis that had greater than 3 counts per cell in at least 10 cells and removing batch-effected genes for G0/G1 bulk RNA-sequencing).

Representation factors were calculated according to (Kim, Lund et al., 2001). The representation factor shows whether genes from one list (list A) are enriched in another list (list B), assuming that genes behave independently.

Acknowledgements

We thank Jon Cooper, Eric Holland, and members of the Paddison lab for helpful discussions, and Do-Hyun Nam, Xiao-Nan Li, Atsushi Miyawaki, and Sabrina Spencer for providing reagents. This work was supported by the following grants: Interdisciplinary Training in Cancer Fellowship NCI T32CA080416 (PH), NCI/NIH (R01CA190957; R21CA170722; P30CA15704) (PP), DoD Translational New Investigator Award CA100735 (PP), and the Pew Biomedical Scholars Program (PP).

Author contributions

Project conception and design was carried out by P.J.P., H.M.F., and C.M.T., CRISPR-Cas9 screening was performed by H.M.F., C.M.T., and P.H., hit validation was performed by H.M.F, C.M.T., P.H., and M.K., critical reagents were generated by P.C. and L.C., screen and RNA-seq data analysis and statistics was performed by S.A. and R.B., sequencing was performed under the supervision of J.D., single cell RNA-sequencing was performed by H.M.F. under supervision of J.L.M.-F. and C.T. and the data analyzed, interpreted, and statistics by C.L.P., H.B. performed cancer mutation analysis, J.M. and F.Z. designed the tiling library, S.M.P. provided and validated the hNPCs, and P.J.P. and H.M.F. wrote the manuscript with input from all authors.

Competing interests

The authors declare no competing interests.

REFERENCES

Anders S, Pyl PT, Huber W (2015) HTSeq--a Python framework to work with high-throughput sequencing data. Bioinformatics 31: 166-9

Arora M, Moser J, Phadke H, Basha AA, Spencer SL (2017) Endogenous Replication Stress in Mother Cells Leads to Quiescence of Daughter Cells. Cell Rep 19: 1351-1364

Artegiani B, Lyubimova A, Muraro M, van Es JH, van Oudenaarden A, Clevers H (2017) A Single-Cell RNA Sequencing Study Reveals Cellular and Molecular Dynamics of the Hippocampal Neurogenic Niche. Cell Rep 21: 3271-3284

Barr AR, Cooper S, Heldt FS, Butera F, Stoy H, Mansfeld J, Novak B, Bakal C (2017) DNA damage during S-phase mediates the proliferation-quiescence decision in the subsequent G1 via p21 expression. Nat Commun 8: 14728

Bergsland M, Werme M, Malewicz M, Perlmann T, Muhr J (2006) The establishment of neuronal properties is controlled by Sox4 and Sox11. Genes Dev 20: 3475-86

Bressan RB, Dewari PS, Kalantzaki M, Gangoso E, Matjusaitis M, Garcia-Diaz C, Blin C, Grant V, Bulstrode H, Gogolok S, Skarnes WC, Pollard SM (2017) Efficient CRISPR/Cas9-assisted gene targeting enables rapid and precise genetic manipulation of mammalian neural stem cells. Development 144: 635-648

Buettner F, Natarajan KN, Casale FP, Proserpio V, Scialdone A, Theis FJ, Teichmann SA, Marioni JC, Stegle O (2015) Computational analysis of cell-to-cell heterogeneity in single-cell RNA-sequencing data reveals hidden subpopulations of cells. Nat Biotechnol 33: 155-60

Calegari F, Huttner WB (2003) An inhibition of cyclin-dependent kinases that lengthens, but does not arrest, neuroepithelial cell cycle induces premature neurogenesis. J Cell Sci 116: 4947-55

Chawla K, Tripathi S, Thommesen L, Laegreid A, Kuiper M (2013) TFcheckpoint: a curated compendium of specific DNA-binding RNA polymerase II transcription factors. Bioinformatics 29: 2519-20

Coats S, Flanagan WM, Nourse J, Roberts JM (1996) Requirement of p27Kip1 for restriction point control of the fibroblast cell cycle. Science 272: 877-80

Cordenonsi M, Zanconato F, Azzolin L, Forcato M, Rosato A, Frasson C, Inui M, Montagner M, Parenti AR, Poletti A, Daidone MG, Dupont S, Basso G, Bicciato S, Piccolo S (2011) The Hippo transducer TAZ confers cancer stem cell-related traits on breast cancer cells. Cell 147: 759-72

Coronado D, Godet M, Bourillot PY, Tapponnier Y, Bernat A, Petit M, Afanassieff M, Markossian S, Malashicheva A, Iacone R, Anastassiadis K, Savatier P (2013) A short G1 phase is an intrinsic determinant of naive embryonic stem cell pluripotency. Stem Cell Res 10: 118-31

Davis AA, Temple S (1994) A self-renewing multipotential stem cell in embryonic rat cerebral cortex. Nature 372: 263-6

Doench JG, Fusi N, Sullender M, Hegde M, Vaimberg EW, Donovan KF, Smith I, Tothova Z, Wilen C, Orchard R, Virgin HW, Listgarten J, Root DE (2016) Optimized sgRNA design to maximize activity and minimize off-target effects of CRISPR-Cas9. Nat Biotechnol 34: 184-191

Doetsch F (2003) A niche for adult neural stem cells. Curr Opin Genet Dev 13: 543-50

El Wakil A, Francius C, Wolff A, Pleau-Varet J, Nardelli J (2006) The GATA2 transcription factor negatively regulates the proliferation of neuronal progenitors. Development 133: 2155-65

Feramisco JR, Gross M, Kamata T, Rosenberg M, Sweet RW (1984) Microinjection of the oncogene form of the human H-ras (T-24) protein results in rapid proliferation of quiescent cells. Cell 38: 109-17

Fischer M (2017) Census and evaluation of p53 target genes. Oncogene 36: 3943-3956

Furutachi S, Matsumoto A, Nakayama KI, Gotoh Y (2013) p57 controls adult neural stem cell quiescence and modulates the pace of lifelong neurogenesis. EMBO J 32: 970-81

Futreal PA, Coin L, Marshall M, Down T, Hubbard T, Wooster R, Rahman N, Stratton MR (2004) A census of human cancer genes. Nat Rev Cancer 4: 177-83

Gil-Perotin S, Marin-Husstege M, Li J, Soriano-Navarro M, Zindy F, Roussel MF, Garcia-Verdugo JM, Casaccia-Bonnefil P (2006) Loss of p53 induces changes in the behavior of subventricular zone cells: implication for the genesis of glial tumors. J Neurosci 26: 1107-16

Gottlieb E, Haffner R, King A, Asher G, Gruss P, Lonai P, Oren M (1997) Transgenic mouse model for studying the transcriptional activity of the p53 protein: age- and tissue-dependent changes in radiation-induced activation during embryogenesis. EMBO J 16: 1381-90

Gray PA, Fu H, Luo P, Zhao Q, Yu J, Ferrari A, Tenzen T, Yuk DI, Tsung EF, Cai Z, Alberta JA, Cheng LP, Liu Y, Stenman JM, Valerius MT, Billings N, Kim HA, Greenberg ME, McMahon AP, Rowitch DH et al. (2004) Mouse brain organization revealed through direct genome-scale TF expression analysis. Science 306: 2255-7

Hahn AT, Jones JT, Meyer T (2009) Quantitative analysis of cell cycle phase durations and PC12 differentiation using fluorescent biosensors. Cell Cycle 8: 1044-52

Homem CC, Repic M, Knoblich JA (2015) Proliferation control in neural stem and progenitor cells. Nat Rev Neurosci 16: 647-59

Ito A, Lai CH, Zhao X, Saito S, Hamilton MH, Appella E, Yao TP (2001) p300/CBP-mediated p53 acetylation is commonly induced by p53-activating agents and inhibited by MDM2. EMBO J 20: 1331-40

Johe KK, Hazel TG, Muller T, Dugich-Djordjevic MM, McKay RD (1996) Single factors direct the differentiation of stem cells from the fetal and adult central nervous system. Genes Dev 10: 3129-40

Johnson NL, Kemp AW, Kotz S (2005) Univariate discrete distributions. Wiley, Hoboken, N.J.

Joo KM, Kim J, Jin J, Kim M, Seol HJ, Muradov J, Yang H, Choi YL, Park WY, Kong DS, Lee JI, Ko YH, Woo HG, Lee J, Kim S, Nam DH (2013) Patient-Specific Orthotopic Glioblastoma Xenograft Models Recapitulate the Histopathology and Biology of Human Glioblastomas In Situ. Cell Rep

Kamentsky L, Jones TR, Fraser A, Bray MA, Logan DJ, Madden KL, Ljosa V, Rueden C, Eliceiri KW, Carpenter AE (2011) Improved structure, function and compatibility for

CellProfiler: modular high-throughput image analysis software. Bioinformatics 27: 1179-80

Kelly DP, Scarpulla RC (2004) Transcriptional regulatory circuits controlling mitochondrial biogenesis and function. Genes Dev 18: 357-68

Kim SK, Lund J, Kiraly M, Duke K, Jiang M, Stuart JM, Eizinger A, Wylie BN, Davidson GS (2001) A gene expression map for Caenorhabditis elegans. Science 293: 2087-92

Komarova EA, Chernov MV, Franks R, Wang K, Armin G, Zelnick CR, Chin DM, Bacus SS, Stark GR, Gudkov AV (1997) Transgenic mice with p53-responsive lacZ: p53 activity varies dramatically during normal development and determines radiation and drug sensitivity in vivo. EMBO J 16: 1391-400

Lange C, Huttner WB, Calegari F (2009) Cdk4/cyclinD1 overexpression in neural stem cells shortens G1, delays neurogenesis, and promotes the generation and expansion of basal progenitors. Cell Stem Cell 5: 320-31

Langmead B, Trapnell C, Pop M, Salzberg SL (2009) Ultrafast and memory-efficient alignment of short DNA sequences to the human genome. Genome Biol 10: R25

Lavado A, He Y, Pare J, Neale G, Olson EN, Giovannini M, Cao X (2013) Tumor suppressor Nf2 limits expansion of the neural progenitor pool by inhibiting Yap/Taz transcriptional coactivators. Development 140: 3323-34

Li X, Floriddia EM, Toskas K, Chalfouh C, Honore A, Aumont A, Vallieres N, Lacroix S, Fernandes KJL, Guerout N, Barnabe-Heider F (2018) FoxJ1 regulates spinal cord development and is required for the maintenance of spinal cord stem cell potential. Exp Cell Res 368: 84-100

Lin H (2008) Cell biology of stem cells: an enigma of asymmetry and self-renewal. J Cell Biol 180: 257-60

Lin JI, Poon CL, Harvey KF (2013) The Hippo size control pathway--ever expanding. Sci Signal 6: pe4

Llorens-Bobadilla E, Zhao S, Baser A, Saiz-Castro G, Zwadlo K, Martin-Villalba A (2015) Single-Cell Transcriptomics Reveals a Population of Dormant Neural Stem Cells that Become Activated upon Brain Injury. Cell Stem Cell 17: 329-40

Macosko EZ, Basu A, Satija R, Nemesh J, Shekhar K, Goldman M, Tirosh I, Bialas AR, Kamitaki N, Martersteck EM, Trombetta JJ, Weitz DA, Sanes JR, Shalek AK, Regev A, McCarroll SA (2015) Highly Parallel Genome-wide Expression Profiling of Individual Cells Using Nanoliter Droplets. Cell 161: 1202-1214

Meletis K, Wirta V, Hede SM, Nister M, Lundeberg J, Frisen J (2006) p53 suppresses the self-renewal of adult neural stem cells. Development 133: 363-9

Miyama S, Takahashi T, Nowakowski RS, Caviness VS, Jr. (1997) A gradient in the duration of the G1 phase in the murine neocortical proliferative epithelium. Cereb Cortex 7: 678-89

Naetar N, Soundarapandian V, Litovchick L, Goguen KL, Sablina AA, Bowman-Colin C, Sicinski P, Hahn WC, DeCaprio JA, Livingston DM (2014) PP2A-mediated regulation of Ras signaling in G2 is essential for stable quiescence and normal G1 length. Mol Cell 54: 932-45

Obernier K, Cebrian-Silla A, Thomson M, Parraguez JI, Anderson R, Guinto C, Rodas Rodriguez J, Garcia-Verdugo JM, Alvarez-Buylla A (2018) Adult Neurogenesis Is Sustained by Symmetric Self-Renewal and Differentiation. Cell Stem Cell 22: 221-234 e8

Plouffe SW, Meng Z, Lin KC, Lin B, Hong AW, Chun JV, Guan KL (2016) Characterization of Hippo Pathway Components by Gene Inactivation. Mol Cell 64: 993-1008

Pollard SM, Conti L, Sun Y, Goffredo D, Smith A (2006) Adherent neural stem (NS) cells from fetal and adult forebrain. Cereb Cortex 16 Suppl 1: i112-20

Pollard SM, Yoshikawa K, Clarke ID, Danovi D, Stricker S, Russell R, Bayani J, Head R, Lee M, Bernstein M, Squire JA, Smith A, Dirks P (2009) Glioma stem cell lines expanded in adherent culture have tumor-specific phenotypes and are suitable for chemical and genetic screens. Cell Stem Cell 4: 568-80

Resnitzky D, Hengst L, Reed SI (1995) Cyclin A-associated kinase activity is rate limiting for entrance into S phase and is negatively regulated in G1 by p27Kip1. Mol Cell Biol 15: 4347-52

Reya T, Morrison SJ, Clarke MF, Weissman IL (2001) Stem cells, cancer, and cancer stem cells. Nature 414: 105-11

Robinson MD, McCarthy DJ, Smyth GK (2010) edgeR: a Bioconductor package for differential expression analysis of digital gene expression data. Bioinformatics 26: 139-40

Sakamoto M, Hirata H, Ohtsuka T, Bessho Y, Kageyama R (2003) The basic helix-loop-helix genes Hesr1/Hey1 and Hesr2/Hey2 regulate maintenance of neural precursor cells in the brain. J Biol Chem 278: 44808-15

Sakaue-Sawano A, Kurokawa H, Morimura T, Hanyu A, Hama H, Osawa H, Kashiwagi S, Fukami K, Miyata T, Miyoshi H, Imamura T, Ogawa M, Masai H, Miyawaki A (2008) Visualizing spatiotemporal dynamics of multicellular cell-cycle progression. Cell 132: 487-98

Sanjana NE, Shalem O, Zhang F (2014) Improved vectors and genome-wide libraries for CRISPR screening. Nat Methods 11: 783-784

Santos A, Wernersson R, Jensen LJ (2015) Cyclebase 3.0: a multi-organism database on cell-cycle regulation and phenotypes. Nucleic Acids Res 43: D1140-4

Scott CE, Wynn SL, Sesay A, Cruz C, Cheung M, Gomez Gaviro MV, Booth S, Gao B, Cheah KS, Lovell-Badge R, Briscoe J (2010) SOX9 induces and maintains neural stem cells. Nat Neurosci 13: 1181-9

Shalem O, Sanjana NE, Hartenian E, Shi X, Scott DA, Mikkelsen TS, Heckl D, Ebert BL, Root DE, Doench JG, Zhang F (2014) Genome-scale CRISPR-Cas9 knockout screening in human cells. Science 343: 84-7

Sherr CJ (1995) D-type cyclins. Trends in biochemical sciences 20: 187-90

Sherr CJ, McCormick F (2002) The RB and p53 pathways in cancer. Cancer Cell 2: 103-12

Singh AM, Chappell J, Trost R, Lin L, Wang T, Tang J, Matlock BK, Weller KP, Wu H, Zhao S, Jin P, Dalton S (2014) Cell-Cycle Control of Developmentally Regulated Transcription Factors Accounts for Heterogeneity in Human Pluripotent Cells. Stem Cell Reports 2: 398

Spencer SL, Cappell SD, Tsai FC, Overton KW, Wang CL, Meyer T (2013) The proliferation-quiescence decision is controlled by a bifurcation in CDK2 activity at mitotic exit. Cell 155: 369-83

Sun Y, Pollard S, Conti L, Toselli M, Biella G, Parkin G, Willatt L, Falk A, Cattaneo E, Smith A (2008) Long-term tripotent differentiation capacity of human neural stem (NS) cells in adherent culture. Mol Cell Neurosci 38: 245-58

Susaki E, Nakayama K, Nakayama KI (2007) Cyclin D2 translocates p27 out of the nucleus and promotes its degradation at the G0-G1 transition. Mol Cell Biol 27: 4626-40

Szklarczyk D, Morris JH, Cook H, Kuhn M, Wyder S, Simonovic M, Santos A, Doncheva NT, Roth A, Bork P, Jensen LJ, von Mering C (2017) The STRING database in 2017: quality-controlled protein-protein association networks, made broadly accessible. Nucleic Acids Res 45: D362-D368

Takahashi T, Nowakowski RS, Caviness VS, Jr. (1995) The cell cycle of the pseudostratified ventricular epithelium of the embryonic murine cerebral wall. J Neurosci 15: 6046-57

The Gene Ontology C (2017) Expansion of the Gene Ontology knowledgebase and resources. Nucleic Acids Res 45: D331-D338

Toledo CM, Ding Y, Hoellerbauer P, Davis RJ, Basom R, Girard EJ, Lee E, Corrin P, Hart T, Bolouri H, Davison J, Zhang Q, Hardcastle J, Aronow BJ, Plaisier CL, Baliga NS, Moffat J, Lin Q, Li XN, Nam DH et al. (2015) Genome-wide CRISPR-Cas9 Screens

Reveal Loss of Redundancy between PKMYT1 and WEE1 in Glioblastoma Stem-like Cells. Cell Rep 13: 2425-2439

Trapnell C, Roberts A, Goff L, Pertea G, Kim D, Kelley DR, Pimentel H, Salzberg SL, Rinn JL, Pachter L (2012) Differential gene and transcript expression analysis of RNA-seq experiments with TopHat and Cufflinks. Nat Protoc 7: 562-78

van Lookeren Campagne M, Gill R (1998) Tumor-suppressor p53 is expressed in proliferating and newly formed neurons of the embryonic and postnatal rat brain: comparison with expression of the cell cycle regulators p21Waf1/Cip1, p27Kip1, p57Kip2, p16Ink4a, cyclin G1, and the proto-oncogene Bax. J Comp Neurol 397: 181-98

Weinberg RA (1995) The retinoblastoma protein and cell cycle control. Cell 81: 323-30

Wey A, Martinez Cerdeno V, Pleasure D, Knoepfler PS (2010) c- and N-myc regulate neural precursor cell fate, cell cycle, and metabolism to direct cerebellar development. Cerebellum 9: 537-47

Wilson KE, Li YW, Yang N, Shen H, Orillion AR, Zhang J (2014) PTPN14 forms a complex with Kibra and LATS1 proteins and negatively regulates the YAP oncogenic function. J Biol Chem 289: 23693-700

Yang HW, Chung M, Kudo T, Meyer T (2017) Competing memories of mitogen and p53 signalling control cell-cycle entry. Nature 549: 404-408

Yao G, Lee TJ, Mori S, Nevins JR, You L (2008) A bistable Rb-E2F switch underlies the restriction point. Nat Cell Biol 10: 476-82

Young MD, Wakefield MJ, Smyth GK, Oshlack A (2010) Gene ontology analysis for RNA-seq: accounting for selection bias. Genome Biol 11: R14

Yu FX, Zhao B, Guan KL (2015) Hippo Pathway in Organ Size Control, Tissue Homeostasis, and Cancer. Cell 163: 811-28

Yu G, He QY (2016) ReactomePA: an R/Bioconductor package for reactome pathway analysis and visualization. Mol Biosyst 12: 477-9

Zetterberg A, Larsson O, Wiman KG (1995) What is the restriction point? Curr Opin Cell Biol 7: 835-42

Zhang N, Bai H, David KK, Dong J, Zheng Y, Cai J, Giovannini M, Liu P, Anders RA, Pan D (2010) The Merlin/NF2 tumor suppressor functions through the YAP oncoprotein to regulate tissue homeostasis in mammals. Dev Cell 19: 27-38

Zhao B, Wei X, Li W, Udan RS, Yang Q, Kim J, Xie J, Ikenoue T, Yu J, Li L, Zheng P, Ye K, Chinnaiyan A, Halder G, Lai ZC, Guan KL (2007) Inactivation of YAP oncoprotein

by the Hippo pathway is involved in cell contact inhibition and tissue growth control. Genes Dev 21: 2747-61

Zheng GX, Terry JM, Belgrader P, Ryvkin P, Bent ZW, Wilson R, Ziraldo SB, Wheeler TD, McDermott GP, Zhu J, Gregory MT, Shuga J, Montesclaros L, Underwood JG, Masquelier DA, Nishimura SY, Schnall-Levin M, Wyatt PW, Hindson CM, Bharadwaj R et al. (2017) Massively parallel digital transcriptional profiling of single cells. Nature communications 8: 14049

Figure 1 - CRISPR-Cas9 Gene Knockout Screens Identify Antiproliferative Genes in Human Neural Progenitor Cells

A Schematic of CRISPR-Cas9 knockout screen design.

B Enrichment of guide DNA following 21 days outgrowth post-selection using GECKO library (Shalem et al., 2014) (n=2).

C Enrichment of sgRNA using GECKO (n=2), Brunello (Doench et al., 2016) (n=3), or a custom-designed retest library (n=4), with U5-NPC or CB660-NPCs at 10 days or 3 weeks post-selection. Colored guides are enriched (z-score>2; green) or depleted (z-score<2; red) with false discovery rate (FDR)<0.05. Statistical source data provided in Table S1.

D Significant overlap between candidate antiproliferative genes and top decile pan-cancer mutated genes (The Cancer Genome Atlas (TCGA); hypergeometric analysis).

E Top candidate antiproliferative genes.

Figure 1

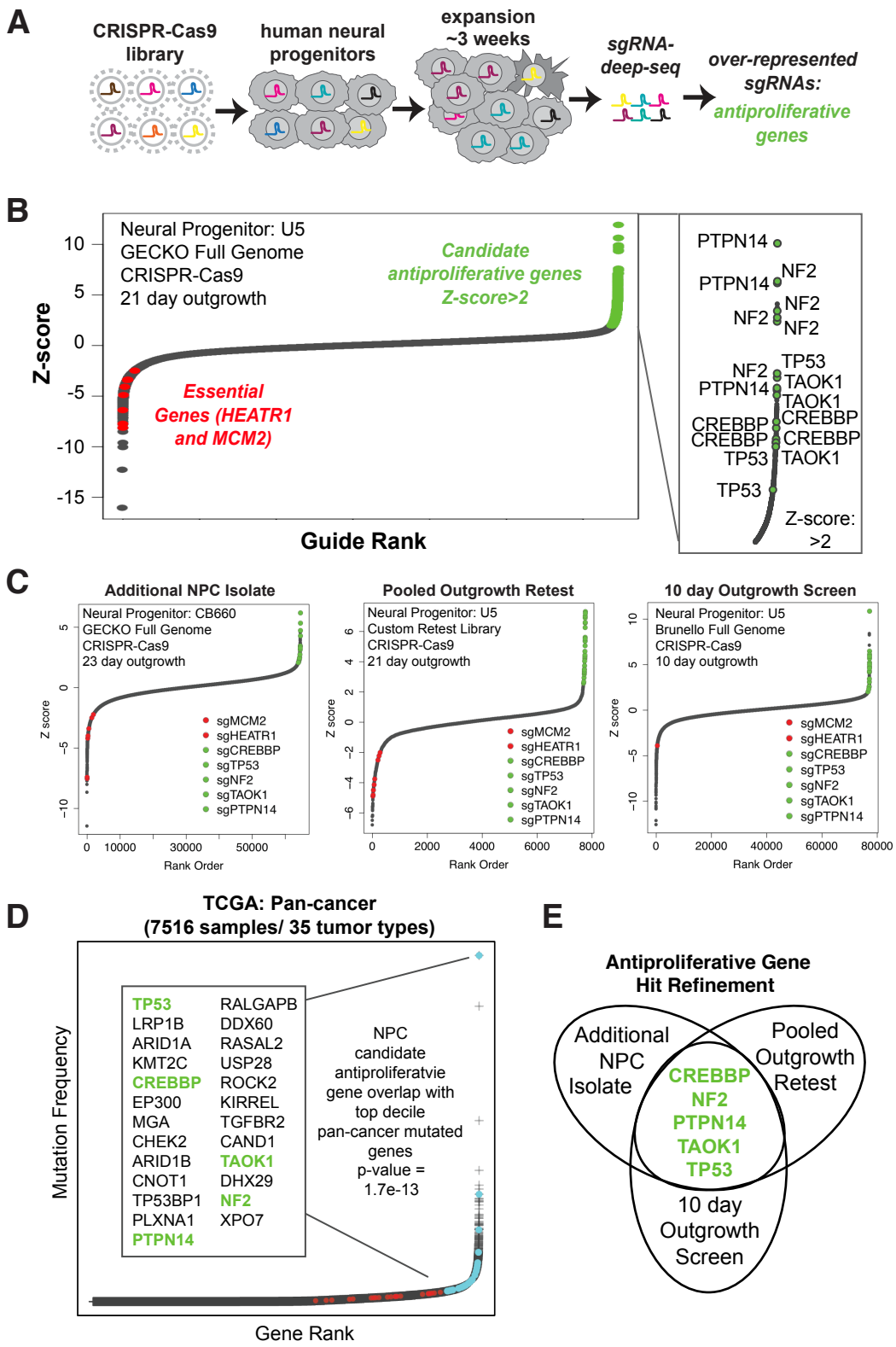
A
CRISPR-Cas9 library
human neural progenitors
expansion ~3 weeks
sgRNA-deep-seq
over-represented sgRNAs:
antiproliferative genes
B
Neural Progenitor: U5
GECKO Full Genome
CRISPR-Cas9
21 day outgrowth
Candidate antiproliferative genes Z-score>2
Essential Genes (HEATR1 and MCM2)
Z-score
Guide Rank
PTPN14
NF2
TP53
TAOK1
CREBBP
Z-score: >2
C
Additional NPC Isolate
Neural Progenitor: CB660
GECKO Full Genome
CRISPR-Cas9
23 day outgrowth
Pooled Outgrowth Retest
Neural Progenitor: U5
Custom Retest Library
CRISPR-Cas9
21 day outgrowth
10 day Outgrowth Screen
Neural Progenitor: U5
Brunello Full Genome
CRISPR-Cas9
10 day outgrowth
sgMCM2
sgHEATR1
sgCREBBP
sgTP53
sgNF2
sgTAOK1
sgPTPN14
Z score
Rank Order
D
TCGA: Pan-cancer
(7516 samples/ 35 tumor types)
Mutation Frequency
TP53
LRP1B
ARID1A
KMT2C
CREBBP
EP300
MGA
CHEK2
ARID1B
CNOT1
TP53BP1
PLXNA1
PTPN14
RALGAPB
DDX60
RASAL2
USP28
ROCK2
KIRREL
TGFBR2
CAND1
TAOK1
DHX29
NF2
XPO7
NPC candidate antiproliferatvie gene overlap with top decile pan-cancer mutated genes p-value = 1.7e-13
Gene Rank
E
Antiproliferative Gene Hit Refinement
Additional NPC Isolate
Pooled Outgrowth Retest
10 day Outgrowth Screen
CREBBP
NF2
PTPN14
TAOK1
TP53

Figure 2 - Validation of *CREBBP*, *NF2*, *PTPN14*, *TAOK1*, and *TP53 as* Antiproliferative Genes in hNPCs

A Enrichment for guides tiled across the coding region for *CREBBP* (n=466), *NF2* (n=138), *PTPN14* (n=263), *TAOK1* (n=141), *TP53* (n=188), and *MCM2* (n=293) and 100 non-targeting controls (TC guides) after 22 days outgrowth in U5-NPCs. Dotted gray line corresponds to the mean of the NTC. Statistical source data provided in Table S1.

B Western blot confirmation of CREBBP and NF2 protein depletion after gene targeting using lentiviral (LV) pools (4 guides/gene) sgRNA:Cas9 after >21 days outgrowth.

C Flow analysis of U5-NPC:GFP with LV-sgRNA:Cas9 retest pools competing with wild-type (WT) U5-NPC over a 23 day outgrowth with ~10% initial proportion (n=3). Competition index refers to the relative increase in %GFP+ compared with initial proportion and mean sgNTC.

D Relative viability of cells, measured through Alamar blue assay, after 7 days outgrowth (n=3).

E Relative confluency of pooled *sgCREBBP* and *sgNF2*, and NTC in U5-NPCs compared to initial confluency over 72 hours at subconfluent density using time lapse microscopy (n=4 sampling regions x 3 biological replicates).

F Representative images of cell confluency at time points 0 and 72h in *LV-sgCREBBP* and sgNF2 treated cells. Scale bars = 150 μm and 50 μm.

G Confluency of cells relative to time=0 in comparison to NTC after 48 hours using time-lapse microscopy (n=4 sampling regions x 3 biological replicates).

H Doubling time measurements (>14 days post-selection) in U5-NPCs or GSCs after 3-5 days outgrowth. n≥3, as noted in bars for each guide.

The data are presented as the mean ± standard deviation (SD). Significance was assessed using a two-tailed student's t test.

Figure 2

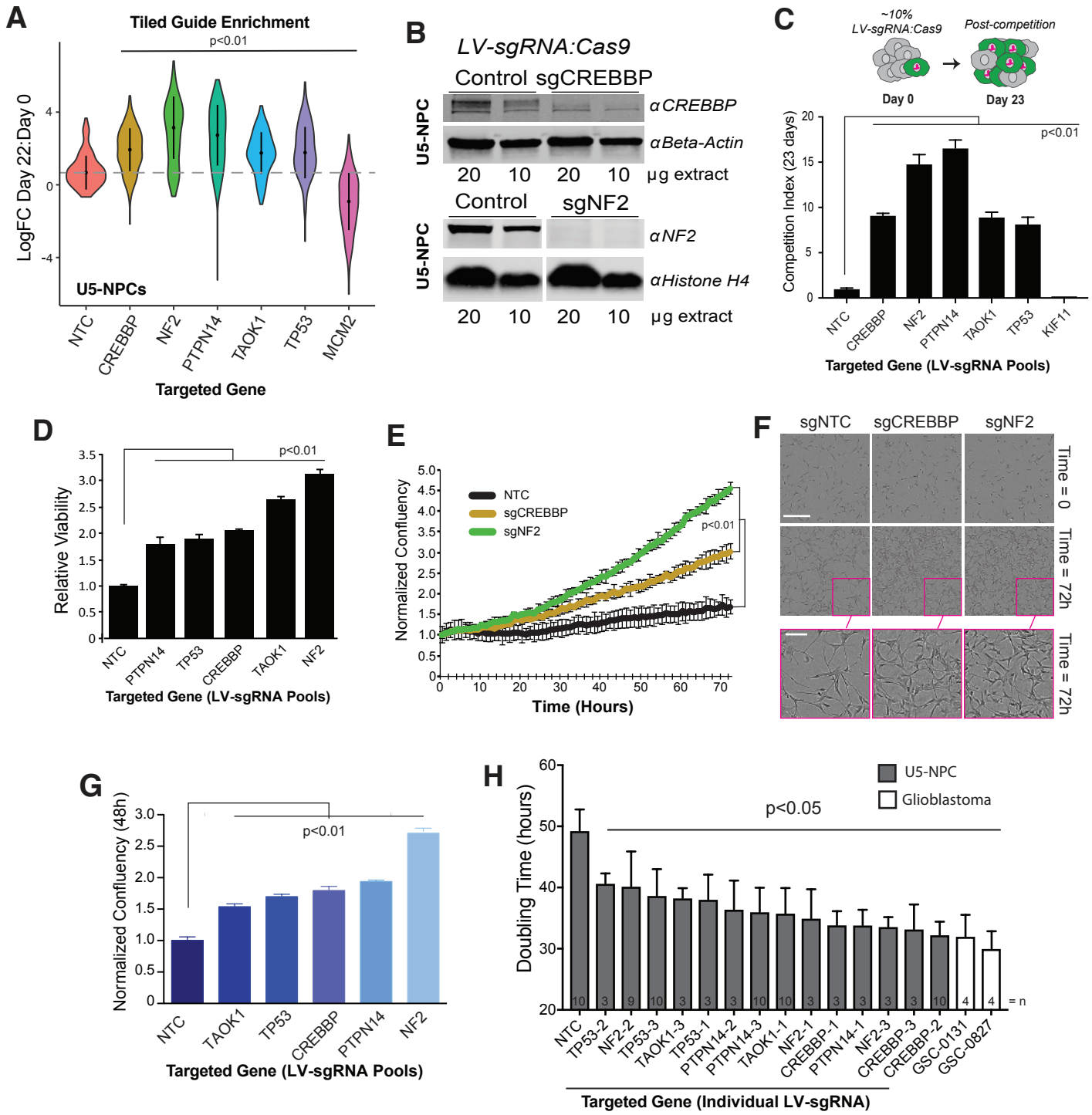
A
Tiled Guide Enrichment
p<0.01
LogFC Day 22:Day 0
U5-NPCs
NTC
CREBBP
NF2
PTPN14
TAOK1
TP53
MCM2
Targeted Gene
B
LV-sgRNA:Cas9
Control
sgCREBBP
U5-NPC
αCREBBP
αBeta-Actin
20 10 20 10 µg extract
Control
sgNF2
αNF2
αHistone H4
20 10 20 10 µg extract
C
~10% LV-sgRNA:Cas9
Post-competition
Day 0
Day 23
Competition Index (23 days)
p<0.01
NTC
CREBBP
NF2
PTPN14
TAOK1
TP53
KIF11
Targeted Gene (LV-sgRNA Pools)
D
Relative Viability
p<0.01
NTC
PTPN14
TP53
CREBBP
TAOK1
NF2
Targeted Gene (LV-sgRNA Pools)
E
Normalized Confluency
NTC
sgCREBBP
sgNF2
p<0.01
Time (Hours)
F
sgNTC
sgCREBBP
sgNF2
Time = 0
Time = 72h
Time = 72h
G
Normalized Confluency (48h)
p<0.01
NTC
TAOK1
TP53
CREBBP
PTPN14
NF2
Targeted Gene (LV-sgRNA Pools)
H
U5-NPC
Glioblastoma
Doubling Time (hours)
p<0.05
NTC
TP53-2
NF2-2
TP53-3
TAOK1-3
TP53-1
PTPN14-2
PTPN14-3
TAOK1-1
NF2-1
CREBBP-1
PTPN14-1
NF2-3
CREBBP-3
CREBBP-2
GSC-0131
GSC-0827
= n
Targeted Gene (Individual LV-sgRNA)

Figure 3 - Reduction of G0/G1 Transit Time in NPCs after KO of *CREBBP*, *NF2*, *PTPN14*, *TAOK1*, or *TP53*

A Representative contour plot of flow cytometry for FUCCI in U5-NPCs after targeting a control gene not affecting proliferation, *GNAS1*. Values are similar to wild-type and NTC U5-NPCs under similar culture conditions. The system relies on cell-cycle dependent degradation of fluorophores using the degrons from CDT1 *(*amino acids (aa) 30-120) (present in G0 and G1; mCherry) and geminin (aa1-110) (present in S, G2, and M; monomeric Azami-Green (mAG)).

B Representative contour maps of flow cytometry for FUCCI following loss of *NF2*, *PTPN14*, *TAOK1*, *CREBBP*, and *TP53*.

C Ratio of G0/G1 (mCherry-CDT1+) to S/G2/M (mAG-Geminin+) from (A) and (B). Values are mean from 4 individually-tested LV guides per gene at 21 days post-selection.

D G0/G1 and S/G2/M transit times using time-lapse microscopy and FUCCI (n=16-60). Differences in G0/G1 are statistically significant with $p<0.0001$ for targeted U5-NPCs and $p=0.0006$ for GSC-0131 compared to NTC.

The data are presented as the mean ± SD. Significance was assessed using a two-tailed student's t test (C) or Mann-Whitney test (D).

Figure 3

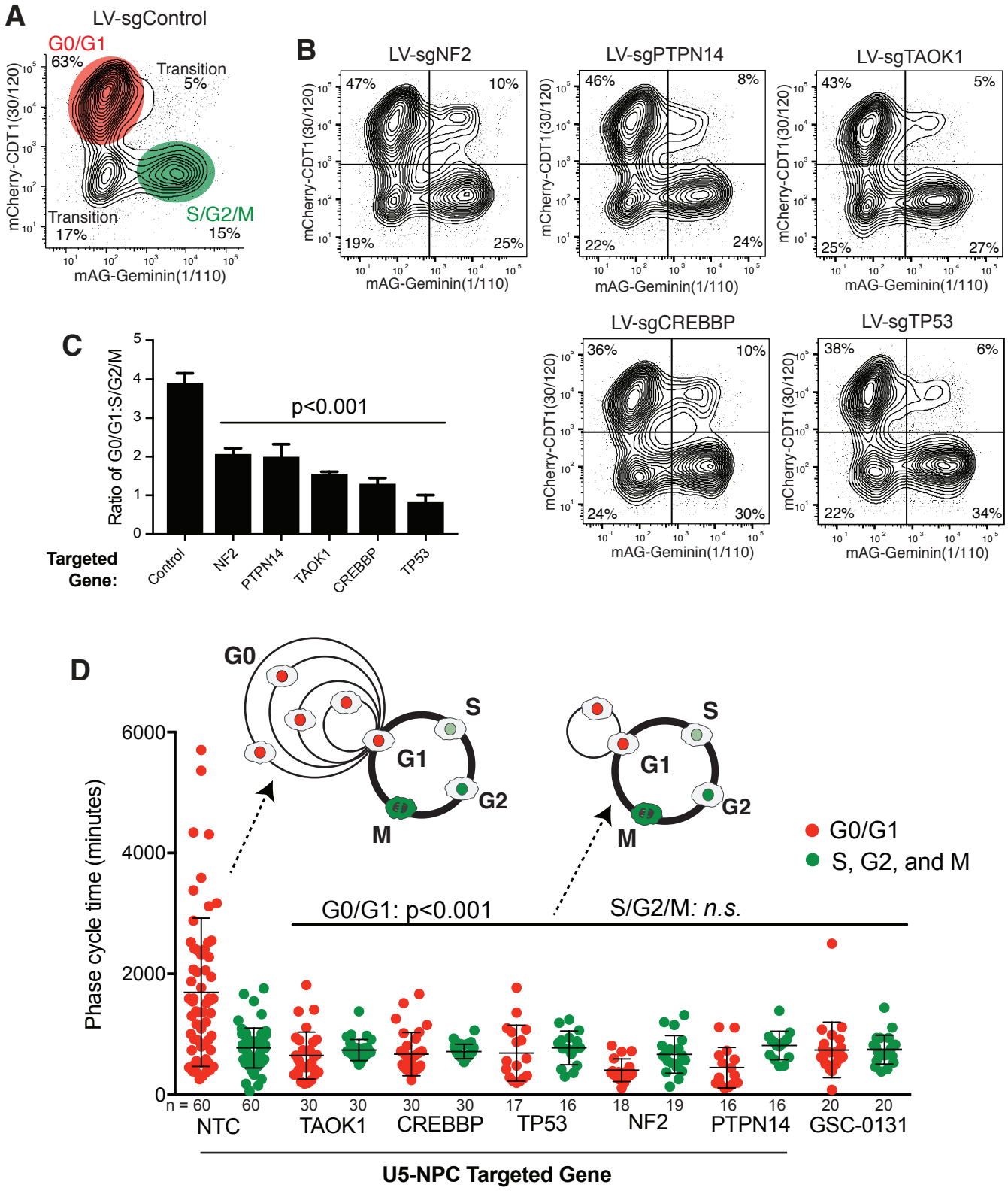
A
LV-sgControl
G0/G1
63%
Transition
5%
Transition
17%
S/G2/M
15%
mCherry-CDT1(30/120)
mAG-Geminin(1/110)
B
LV-sgNF2
47%
10%
19%
25%
LV-sgPTPN14
46%
8%
22%
24%
LV-sgTAOK1
43%
5%
25%
27%
LV-sgCREBBP
36%
10%
24%
30%
LV-sgTP53
38%
6%
22%
34%
C
Ratio of G0/G1:S/G2/M
p<0.001
Targeted Gene:
Control
NF2
PTPN14
TAOK1
CREBBP
TP53
D
G0
S
G1
G2
M
Phase cycle time (minutes)
G0/G1
S, G2, and M
G0/G1: p<0.001
S/G2/M: n.s.
n = 60
60
30
30
30
30
17
16
18
19
16
16
20
20
NTC
TAOK1
CREBBP
TP53
NF2
PTPN14
GSC-0131
U5-NPC Targeted Gene

Figure 4 - Loss of G0-skip Genes Reduces G0 and Increases Late G1 Molecular Features

A Diagram of key molecular features for G0/G1 subpopulations.

B Intensity of immunofluorescence staining for phosphorylated Rb (Ser807/811) in G0/G1 U5-NPCs (mCherry-CDT1+) (Median ± SD; n=2456-8048 cells).

C CDK2 activity in G0/G1 hNPCs after KO measured through the relative ratio of a DNA helicase B (DHB) reporter (Hahn et al., 2009) using fluorescence microscopy. G0/G1 nuclei were identified by the presence of mCherry-CDT1 and due to the irregular shape of the NPCs, the cytoplasmic intensity of the DHB reporter was defined as the upper quartile intensity of a 2-pixel ring around the CDT1-defined nucleus (n=960-8048 cells). NF2 KO was not significantly different from NTC (p=0.51).

D Proportion of G0/G1 cells with cytoplasmic:nuclear ratio >1 for CDK2 activity reporter (n=54 fields).

E Representative distribution of the entire population of U5-NPCs for p27K^{-}-mVenus assayed using flow cytometry after KO along with WT and NTC. Threshold to define p27^{high} set at the top ~10% of the NTC for each independent replicate.

F Proportion of cells p27^{high} following KO, assayed using flow cytometry (n=3).

G Model for the changes in G0/G1 molecular features following loss of *CREBBP*, *NF2*, *PTPN14*, *TAOK1*, or *TP53*.

The data are presented as the mean ± SD. Significance was assessed using a two-tailed student's t test.

Figure 4

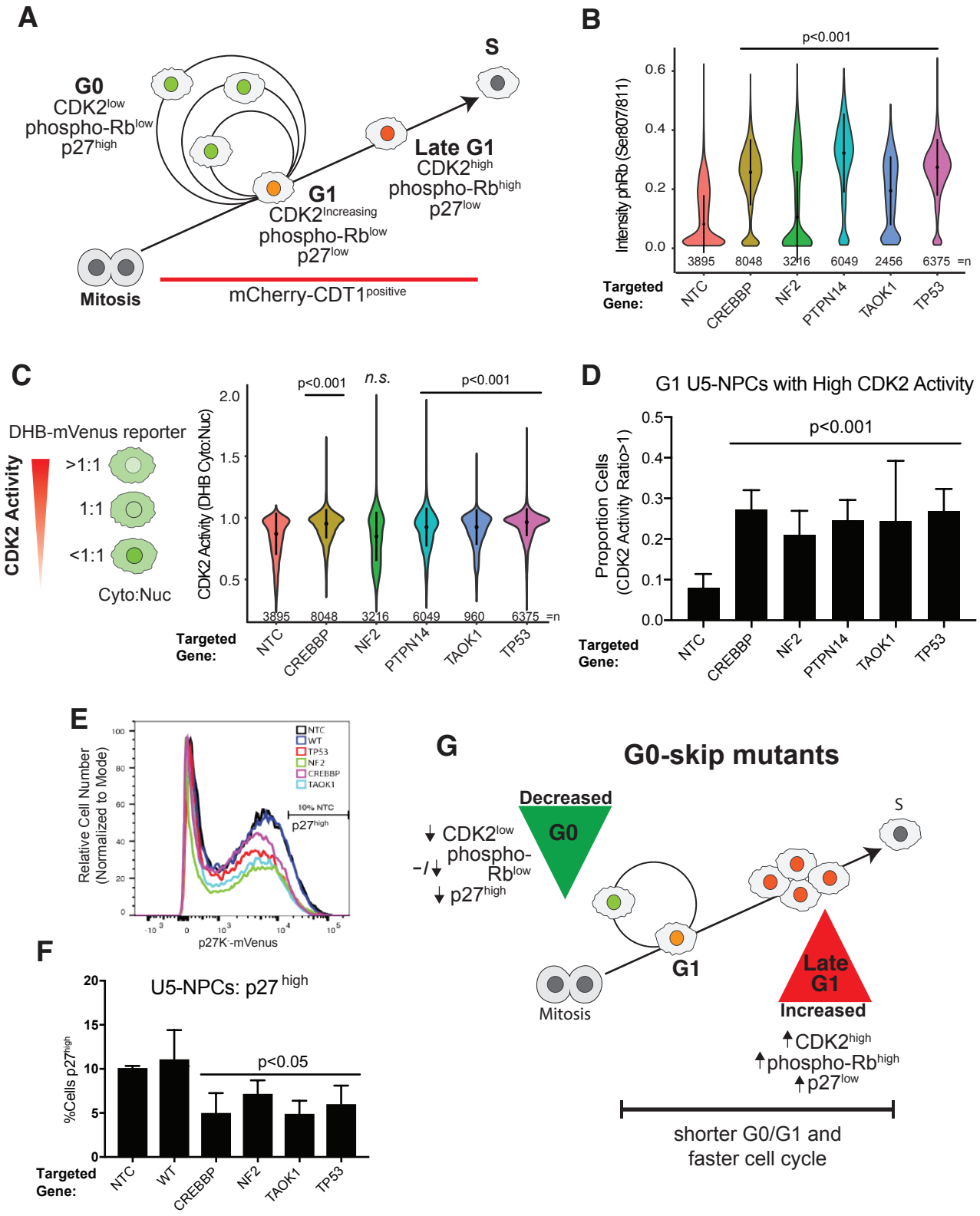
A
G0
CDK2low
phospho-Rblow
p27high
S
Late G1
CDK2high
phospho-Rbhigh
p27low
G1
CDK2Increasing
phospho-Rblow
p27low
Mitosis
mCherry-CDT1positive
B
p<0.001
Intensity phRb (Ser807/811)
3895 8048 3216 6049 2456 6375 =n
Targeted Gene:
NTC CREBBP NF2 PTPN14 TAOK1 TP53
C
DHB-mVenus reporter
CDK2 Activity
>1:1
1:1
<1:1
Cyto:Nuc
p<0.001
n.s.
p<0.001
CDK2 Activity (DHB Cyto:Nuc)
3895 8048 3216 6049 960 6375 =n
Targeted Gene:
NTC CREBBP NF2 PTPN14 TAOK1 TP53
D
G1 U5-NPCs with High CDK2 Activity
p<0.001
Proportion Cells (CDK2 Activity Ratio>1)
Targeted Gene:
NTC CREBBP NF2 PTPN14 TAOK1 TP53
E
Relative Cell Number (Normalized to Mode)
NTC
WT
TP53
NF2
CREBBP
TAOK1
10% NTC
p27high
p27K-mVenus
F
U5-NPCs: p27 high
%Cells p27high
p<0.05
Targeted Gene:
NTC WT CREBBP NF2 TAOK1 TP53
G
G0-skip mutants
Decreased
G0
↓ CDK2low
-/↓ phospho-Rblow
↓ p27high
S
G1
Mitosis
Late G1
Increased
↑CDK2high
↑phospho-Rbhigh
↑p27low
shorter G0/G1 and faster cell cycle

Figure 5 - Transcriptional Reprogramming of G0/G1 Following Loss of G0-skip Genes

A Schematic of G0/G1 sorting for gene expression analysis: mCherry-CDT1+ U5-NPCs (red box), heat maps of the significantly altered genes (FDR<0.05) between WT unsorted U5-NPCs and NTC and WT G0/G1 U5-NPCs, and gene ontology analysis (Young et al., 2010) of some of the top biological processes down-regulated and reactome groups (Yu & He, 2016) up-regulated in the G0/G1 sorted cells. Full list in Table S2.

B Dendrogram of unbiased hierarchical clustering of gene expression from G0/G1-sorted U5-NPCs with the number genes up (green) and down (red) regulated (FDR<0.05) in each KO compared to NTC. Complete results in Table S2.

C Heat map of $\log_2$FC compared to NTC for key genes changed in G0/G1 in following loss of *TP53, NF2/PTPN14*, *TAOK1*, and/or *CREBBP*, including genes from TP53 targets, YAP targets, the cell cycle, Hippo signaling, and electron transport genes. White dots indicate FDR<0.05.

D,E Overlap of a selection of biological process enriched in up (D) and down (E) regulated genes in G0/G1 following KO of G0-skip genes using gene ontology analysis. Full list in Table S3.

Figure 5

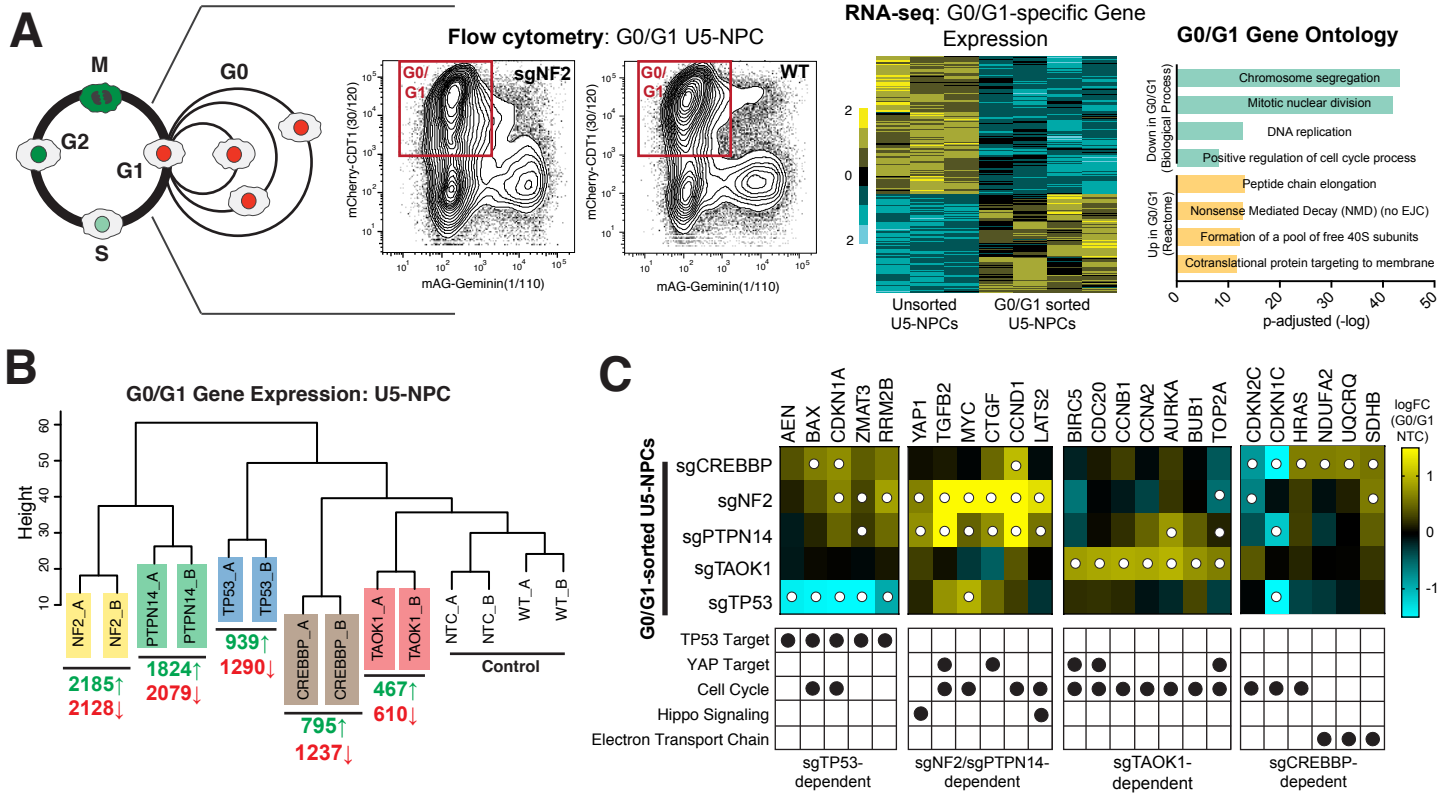
A
M
G0
G2
G1
S
Flow cytometry: G0/G1 U5-NPC
G0/G1
sgNF2
WT
mCherry-CDT1(30/120)
mAG-Geminin(1/110)
RNA-seq: G0/G1-specific Gene Expression
Unsorted U5-NPCs
G0/G1 sorted U5-NPCs
G0/G1 Gene Ontology
Down in G0/G1 (Biological Process)
Up in G0/G1 (Reactome)
Chromosome segregation
Mitotic nuclear division
DNA replication
Positive regulation of cell cycle process
Peptide chain elongation
Nonsense Mediated Decay (NMD) (no EJC)
Formation of a pool of free 40S subunits
Cotranslational protein targeting to membrane
p-adjusted (-log)
B
G0/G1 Gene Expression: U5-NPC
Height
NF2_A
NF2_B
PTPN14_A
PTPN14_B
TP53_A
TP53_B
CREBBP_A
CREBBP_B
TAOK1_A
TAOK1_B
NTC_A
NTC_B
WT_A
WT_B
Control
2185↑
2128↓
1824↑
2079↓
939↑
1290↓
795↑
1237↓
467↑
610↓
C
AEN
BAX
CDKN1A
ZMAT3
RRM2B
YAP1
TGFB2
MYC
CTGF
CCND1
LATS2
BIRC5
CDC20
CCNB1
CCNA2
AURKA
BUB1
TOP2A
CDKN2C
CDKN1C
HRAS
NDUFA2
UQCRQ
SDHB
logFC (G0/G1 NTC)
G0/G1-sorted U5-NPCs
sgCREBBP
sgNF2
sgPTPN14
sgTAOK1
sgTP53
TP53 Target
YAP Target
Cell Cycle
Hippo Signaling
Electron Transport Chain
sgTP53-dependent
sgNF2/sgPTPN14-dependent
sgTAOK1-dependent
sgCREBBP-depedent
D
Up-regulated Genes (G0/G1-sorted): Biological Processes
sgTAOK1
sgTP53
sgCREBBP
sgPTPN14
sgNF2
mitotic nuclear division
chromosome segregation
extracellular structure organization
extracellular matrix organization
energy derivation by oxidation of organic compounds
response to tumor necrosis factor
respiratory electron transport chain
endoplasmic reticulum unfolded protein response
blood vessel morphogenesis
cell junction organization
regulation of vesicle-mediated transport
epithelial cell development
hippo signaling
positive regulation of cell motility
response to oxygen levels
response to transforming growth factor beta
Wnt signaling pathway
mesenchymal cell development
transforming growth factor beta production
regulation of extent of cell growth
E
Down-regulated Genes (G0/G1-sorted): Biological Processes
sgTAOK1
sgTP53
sgCREBBP
sgPTPN14
sgNF2
axon development
positive regulation of neurogenesis
negative regulation of neurogenesis
glial cell differentiation
regulation of membrane potential
response to transforming growth factor beta
Wnt signaling pathway
regulation of neural precurser cell proliferation
establishment or maintenance of apical/basal cell polarity
intrinsic apoptotic signaling by p53 class mediator
oligodendrocyte differentiation
positive regulation of neuron differentiation
dendrite development
smoothened signaling pathway
synapse organization
cilium organization

Figure 6 - Gene Expression Map of Cell Cycle and Candidate G0 and G1 Subpopulations using Single Cell RNA-seq in hNPCs

A Transcriptional clusters of unsorted U5-NPCs derived through an unbiased shared nearest neighbor (SNN) modularity and visualized through a t-Distributed Stochastic Neighbor Embedding (tSNE) comparison. Clusters characterized within the cell cycle based on the analysis in Figs S5,S6, as well as this figure.

B Proportion of cells found in each cluster for the WT U5-NPCs and classification of G0/G1 status according to Fig S5B.

C Heat map of the relative expression (row-wise z-score) for the top 10 non-redundant genes for each prominent cluster in WT U5-NPCs and gene ontology analysis of the up-regulated genes defining each cluster. BP = biological process; R = Reactome; MF = molecular function; CC = cellular component; n/a = non-applicable (gene list derived in this paper). Featured gene ontology groups selected based on significance (p-adj.<.01), representation, and/or non-redundancy. Full cluster-defining gene list is in Supplementary Table 4 and full gene ontology and reactome analysis is in Table S5.

D Network derived from Canberra distance measures shows connections between the cell cycle clusters.

E Model of the cell cycle of cultured hNPCs based on single cell transcriptomes.

F Overlap of the Neural G0 cluster with single cell transcriptomic profiles of quiescent neural stem cells (qNSCs) and activated (a) NSCs/neural progenitors from adult rodent hippocampal niche (Artegiani et al., 2017, Llorens-Bobadilla et al., 2015). Significance assessed using hypergeometric analysis. OPC = oligodendrocyte progenitor.

Figure 6

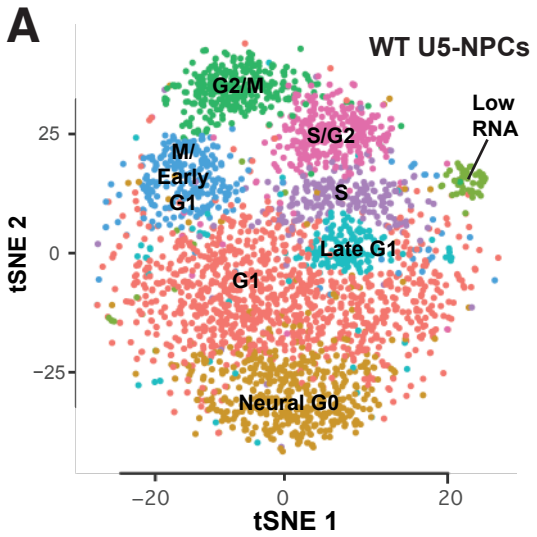

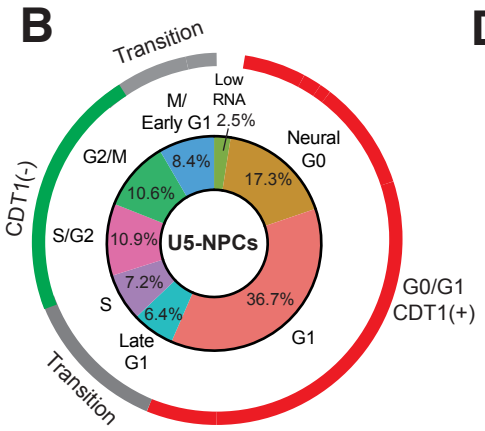

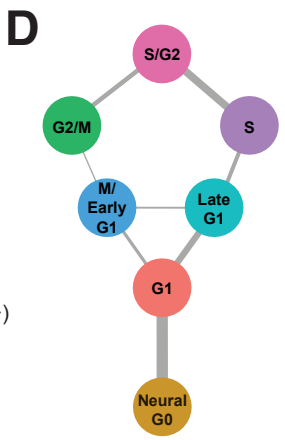

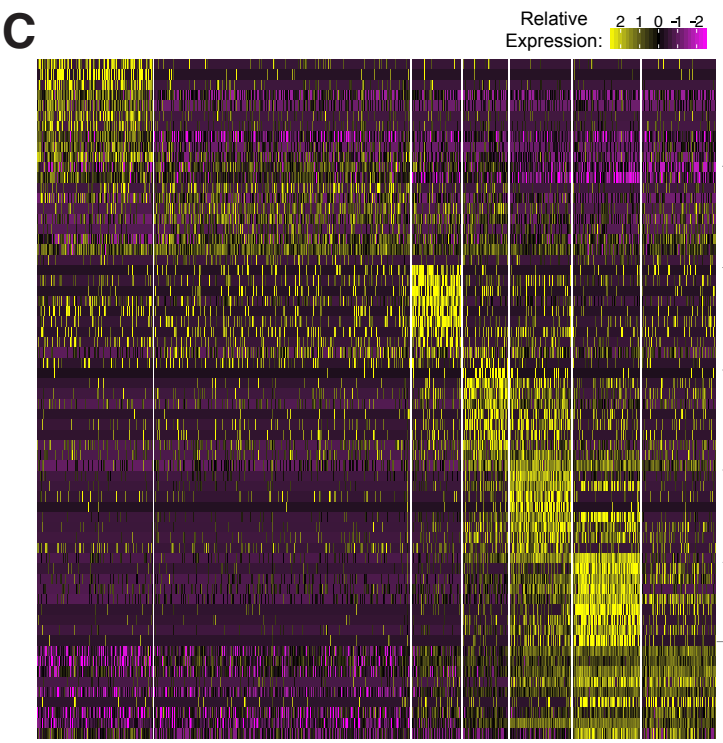

	Top Cluster-defining Genes		Gene Ontology Groups	Category	p-adj.
Neural G0	SCRG1 PLP1 S100B GPM6B BEX1	PTPRZ1 PRCP PTN SOX4 SAT1	Glial cell differentiation Oligodendrocyte differentiation	BP BP	5.7E-06 2.5E-03
G1	IGFBP3 IGFBP5 MIAT MAP3K7CL AHNAK2	TPST2 DLG1 CMTM7 C6orf15 GJB2	(+) regulation of IGF1R signaling Epithelial cell proliferation	BP BP	6.4E-03 6.4E-03
Late G1	EDN1 CYR61 ANKRD1 CTGF PLK2	PLK2 UGCG ARID5B PLAU CCL2	Cholesterol biosynthesis Cadherin binding (cell-cell adhesion) Conserved YAP (NF2) targets	R MF n/a	1.8E-14 3.1E-03 3.1E-09
S	CCNE2 CLSPN GINS2 PCNA ATAD2	MCM7 MCM3 SLBP GMNN KIAA0101	DNA replication S phase G1/S Transition	BP R R	5.6E-31 2.7E-19 8.8E-19
S/G2	HIST1H4C CDK1 HIST1H1E HIST1H1B UBE2C	RRM2 ZWINT HIST1H1C HMGB2	Mitotic nuclear division Condensed chromosome DNA replication	BP CC BP	3.5E-37 3.2E-28 3.7E-18
G2/M	CCNB1 CENPF CKS2 PTTG1	CDC20 TOP2A NUSAP1 CENPA	Mitotic nuclear division Spindle	BP CC	8.8E-63 1.4E-46
M/Early G1	HMGN2 TUBA1B STMN1 BIRC5 HMGB1	TROAP HNRNPA2B1 H2AFZ ARL6IP1	Spliceosomal complex RNA splicing Mitotic nuclear division	CC BP BP	3.2E-06 4.3E-06 5.9E-04

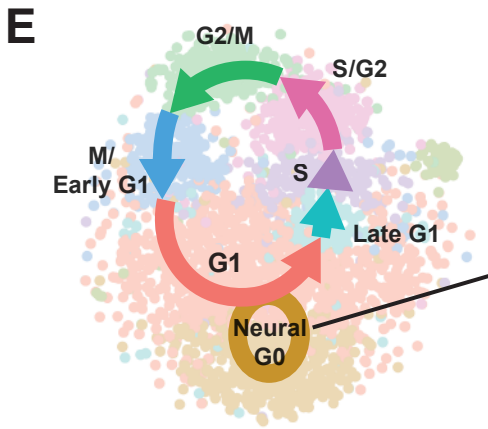

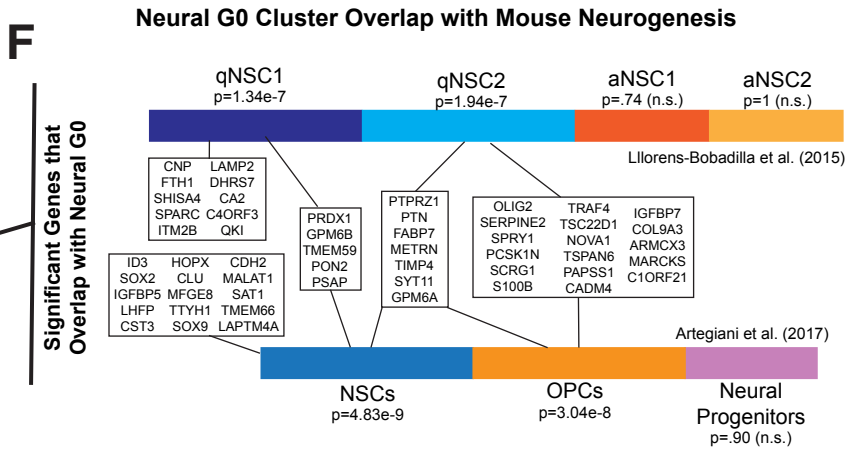

Figure 7 - Loss of G0-skip Genes Alters G0/G1 Subpopulations and Modulates Differentiation and Lineage Specification in hNPCs

A,B Significance of overlap of the down (A) and up (B) regulated genes from bulk RNA-sequencing of G0/G1 sorted cells with the single cell cluster definitions (up-regulated genes). Significance assessed though hypergeometric analysis. RF = representation factor.

C,D tSNE plots and relative cluster proportions from G0/G1 sorted (FUCCI CDT1+) U5-NPCs (WT (C) and sgTAOK1 (D)) characterized based on cell cycle cluster definitions.

E Cell cycle clusters that are significantly different in G0/G1 sgTAOK1 vs. G0/G1 WT U5-NPCs after single cell RNA-sequencing. Significance was assessed using the proportion test.

F Relative expression of early NPC differentiation lineage specification modules based on the gene ontology groups up-regulated in NTC U5-NPCs following 1 week differentiation through mitogenic growth factor (GF) withdrawal. The data are presented as the mean ± standard error of the mean (SEM). Significance was assessed using a two-tailed student's t test. Full analysis in Table S6.

G Heat map of key cell cycle genes that are differentially expressed from NTC U5-NPCs after 1 week differentiation through GF withdrawal. White dots indicate FDR<0.05. Full analysis in Table S7.

H A general model for G0-skipping, highlighting some of the possible mechanisms that would result in skipping G0, including altered cell cycle gene expression.

Figure 7

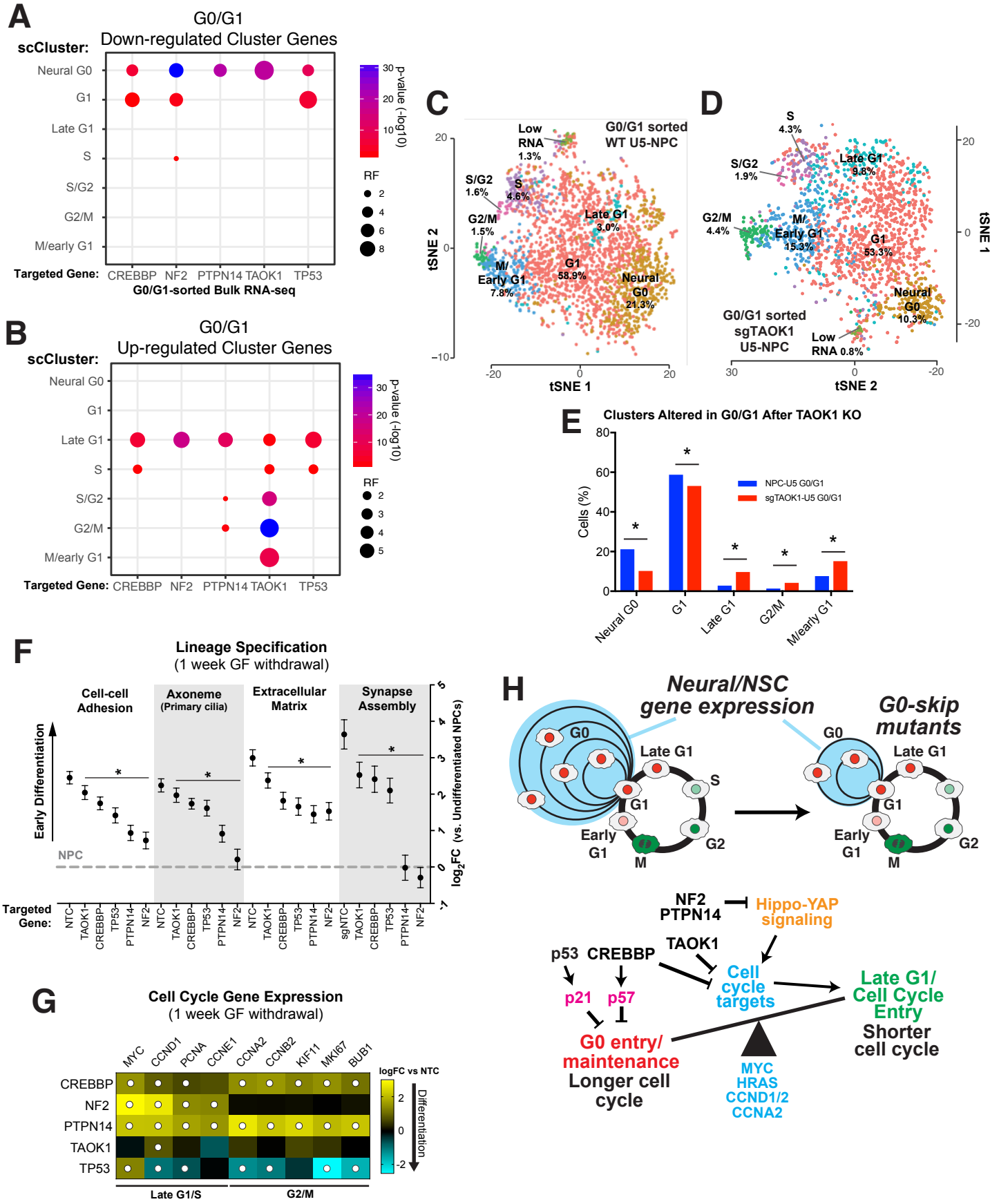
A
G0/G1
Down-regulated Cluster Genes
scCluster:
Neural G0
G1
Late G1
S
S/G2
G2/M
M/early G1
Targeted Gene: CREBBP NF2 PTPN14 TAOK1 TP53
G0/G1-sorted Bulk RNA-seq
p-value (-log10)
RF
B
G0/G1
Up-regulated Cluster Genes
C
G0/G1 sorted
WT U5-NPC
tSNE 1
tSNE 2
D
G0/G1 sorted
sgTAOK1
U5-NPC
E
Clusters Altered in G0/G1 After TAOK1 KO
Cells (%)
NPC-U5 G0/G1
sgTAOK1-U5 G0/G1
F
Lineage Specification
(1 week GF withdrawal)
Cell-cell Adhesion
Axoneme (Primary cilia)
Extracellular Matrix
Synapse Assembly
Early Differentiation
NPC
log2FC (vs. Undifferentiated NPCs)
Targeted Gene:
G
Cell Cycle Gene Expression
(1 week GF withdrawal)
MYC
CCND1
PCNA
CCNE1
CCNA2
CCNB2
KIF11
MKI67
BUB1
CREBBP
NF2
PTPN14
TAOK1
TP53
logFC vs NTC
Differentiation
Late G1/S
G2/M
H
Neural/NSC gene expression
G0-skip mutants
G0
Late G1
S
G1
Early G1
G2
M
NF2
PTPN14
Hippo-YAP signaling
TAOK1
p53
CREBBP
p21
p57
Cell cycle targets
Late G1/ Cell Cycle Entry
Shorter cell cycle
G0 entry/ maintenance
Longer cell cycle
MYC
HRAS
CCND1/2
CCNA2

Supplemental Data Inventory

SUPPLEMENTARY FIGURES

Figure S1: CRISPR-Cas9 Gene Knockout Screens
Identify hNPC Candidate Antiproliferative Genes; Effect is Diminished in Glioblastoma Tumor Isolates.

Figure S2: Validation as Antiproliferative Genes and Knockout Cell Cycle Characterization of CREBBP, NF2, PTPN14, TAOK1, and TP53 in hNPCs.

Figure S3: Transcriptional Target and Cell Cycle Gene Expression Following Loss of G0-skip Genes.

Figure S4: Gene Ontology Analysis of Transcriptional Reprogramming Following Loss of G0-skip Genes.

Figure S5. Identification and Analysis of Cell Cycle Subpopulations from Single Cell RNA-sequencing Unbiased Clustering.

Figure S6: Further Analysis of Cell Cycle Subpopulations from Single Cell RNA-sequencing and Comparison to Other Datasets.

Figure S7: Altered Expression of Single-Cell Cell Cycle Cluster Definition Genes in Bulk RNA-sequencing Datasets and Differentiation in G0-skip Mutants.

SUPPLEMENTARY TABLES

Table S1: CRISPR-Cas9 Screens to Identify and Validate Antiproliferative Genes in Human Neural Progenitor Cells.

Table S2: Gene Expression of G0/G1-sorted Cells Compared to Unsorted U5-NPCs, after G0-skip KO, and in GSC Isolates.

Table S3: Biological Process Gene Ontology Analysis of G0/G1 Transcriptional Reprogramming in U5-NPCs Following Loss of G0-skip Genes**.**

Table S4: Enriched and Depleted Genes in Cell Cycle Clusters Identified by Single-cell RNA-seq in U5-hNPCs.

Table S5: Gene Ontology Analysis of Defining Genes in Transcriptional Cell Cycle Clusters in U5-NPCs.

Table S6: Gene Expression and Ontology in Early Differentiation after 1 Week Growth Factor Withdrawal in U5-NPCs.

Table S7: Gene Expression and Biological Process Ontology after G0-skip gene KO compared to NTC During Early Differentiation (1 Week Growth Factor Withdrawal).

Table S8: List of Key Resources Including Antibodies, Validation sgDNA Sequences, and Primers

PRIMARY SCREEN AND GENE EXPRESSION DATA

NCBI Gene Expression Omnibus GSE117004 (Token = wvijeqcivtcbdop**)**

Figure S1 - CRISPR-Cas9 Gene Knockout Screens Identify hNPC Candidate Antiproliferative Genes; Effect is Diminished in Glioblastoma Tumor Isolates.

A Overlap of screen hits between the four CRISPR-Cas9 screens. For all screens, hits were defined as genes having multiple guides with FDR<.01 and z-score>2. For Brunello library, there were additional requirements of at least one guide with z-score>3 and at least 20 reads at Day 0. CREBBP, NF2, PTPN14, TAOK1, and TP53 were defined as hits in every screen. Specificity to one of the NPC isolates was only defined if the same library was tested in both isolates.

B Overlap of the candidate antiproliferative genes with validated tumor suppressors (Futreal et al., 2004) (Tier 1 and 2; Cancer Gene Census v84). Significance assessed using hypergeometric analysis.

C Scatterplot of guides in U5-NPCs, GSC-0131 (n=5), GSC-0827 (n=5), and GSC-1502 (n=5) with a positive log_2FC (logFC) following ~3 weeks outgrowth post-selection following transduction with a custom CRISPR-Cas9 retest library. Dots for individual guides were colored only if significant (sig) (FDR<0.05 and logFC>1). Loss of the proliferation-limiting genes has a more limited effect in GSCs compared to NPCs in both magnitude and number of significant guides.

Figure S1

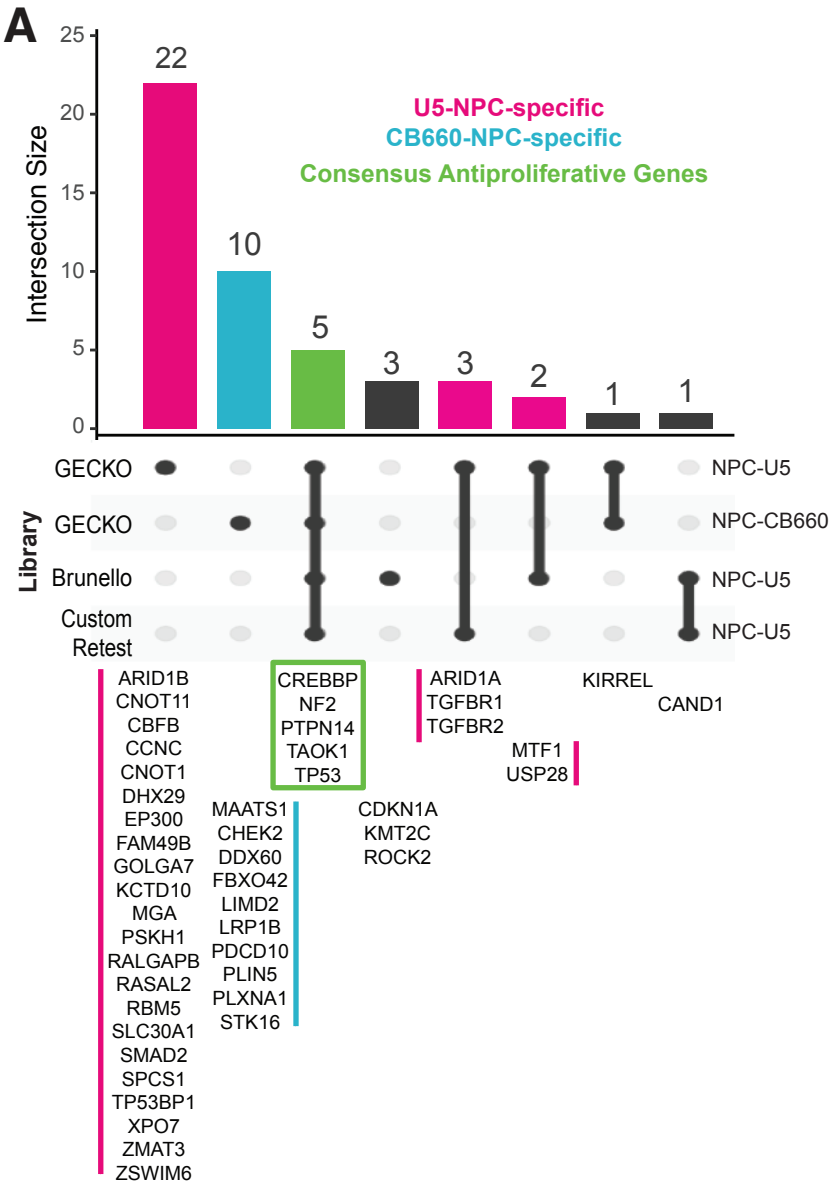
A
Intersection Size
25
20
15
10
5
0
22
10
5
3
3
2
1
1
U5-NPC-specific
CB660-NPC-specific
Consensus Antiproliferative Genes
Library
GECKO
GECKO
Brunello
Custom Retest
NPC-U5
NPC-CB660
NPC-U5
NPC-U5
ARID1B
CNOT11
CBFB
CCNC
CNOT1
DHX29
EP300
FAM49B
GOLGA7
KCTD10
MGA
PSKH1
RALGAPB
RASAL2
RBM5
SLC30A1
SMAD2
SPCS1
TP53BP1
XPO7
ZMAT3
ZSWIM6
CREBBP
NF2
PTPN14
TAOK1
TP53
MAATS1
CHEK2
DDX60
FBXO42
LIMD2
LRP1B
PDCD10
PLIN5
PLXNA1
STK16
CDKN1A
KMT2C
ROCK2
ARID1A
TGFBR1
TGFBR2
MTF1
USP28
KIRREL
CAND1

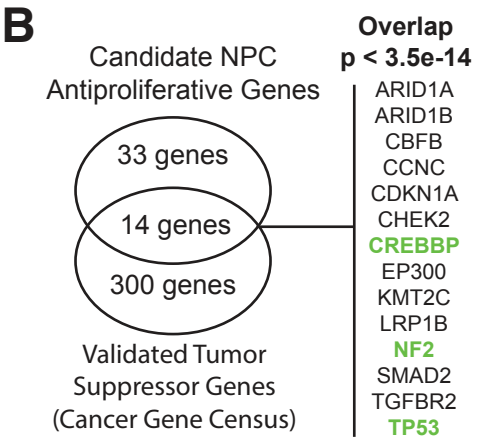
B
Candidate NPC Antiproliferative Genes
33 genes
14 genes
300 genes
Validated Tumor Suppressor Genes (Cancer Gene Census)
Overlap
p < 3.5e-14
ARID1A
ARID1B
CBFB
CCNC
CDKN1A
CHEK2
CREBBP
EP300
KMT2C
LRP1B
NF2
SMAD2
TGFBR2
TP53

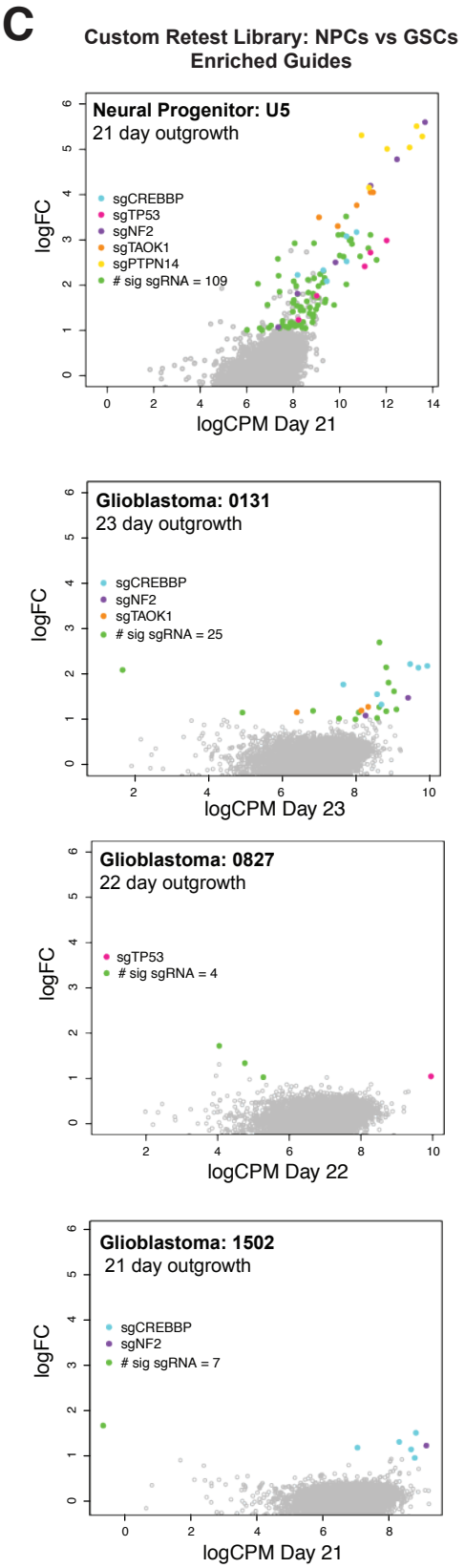
C
Custom Retest Library: NPCs vs GSCs
Enriched Guides
Neural Progenitor: U5
21 day outgrowth
sgCREBBP
sgTP53
sgNF2
sgTAOK1
sgPTPN14
sig sgRNA = 109
logFC
logCPM Day 21
Glioblastoma: 0131
23 day outgrowth
sgCREBBP
sgNF2
sgTAOK1
sig sgRNA = 25
logFC
logCPM Day 23
Glioblastoma: 0827
22 day outgrowth
sgTP53
sig sgRNA = 4
logFC
logCPM Day 22
Glioblastoma: 1502
21 day outgrowth
sgCREBBP
sgNF2
sig sgRNA = 7
logFC
logCPM Day 21

Figure S2 - Validation as Antiproliferative Genes and Knockout Cell Cycle Characterization of *CREBBP*, *NF2*, *PTPN14*, *TAOK1*, and *TP53* in hNPCs.

A Enrichment for guides tiled across the coding region for CREBBP (Exons 1-29; NM_001079846), NF2 (NM_016418), PTPN14 (NM_005401), TAOK1 (NM_020791), TP53 (NM_000546), and MCM2 (NM_004526) after 22 days outgrowth in U5-NPCs. Exons indicated by gold bars. Individual guides are represented by dots with significant guides (FDR<0.05) colored red if depleted (logFC<1) and green if enriched (logFC>1).

B-E The complete cell cycle of individual U5-NPCs expressing FUCCI factors that combine cell cycle-dependent degrons with fluorophores. mCherry-CDT1(aa30-120) (red) is present in G0/G1 and mAG-geminin(aa1-110) (green) is present in S/G2/M. The double negative cells correspond to either a transition state between M and G1 or G1 and S phase or cells that have silenced one or both reporters. Double positive cells which express both CDT1 and Geminin are an alternative G1-S transition state but are rare in the U5-NPC isolate. We tracked individual cells from mitosis to mitosis using timelapse microscopy, every 10-15 minutes, and representative cells from long-cycling NTC (B), short-cycling NTC (C), sgCREBBP (4 guide lentiviral pool) (D), and sgTAOK1 (4 guide lentiviral pool) (E) are presented here.

Figure S2

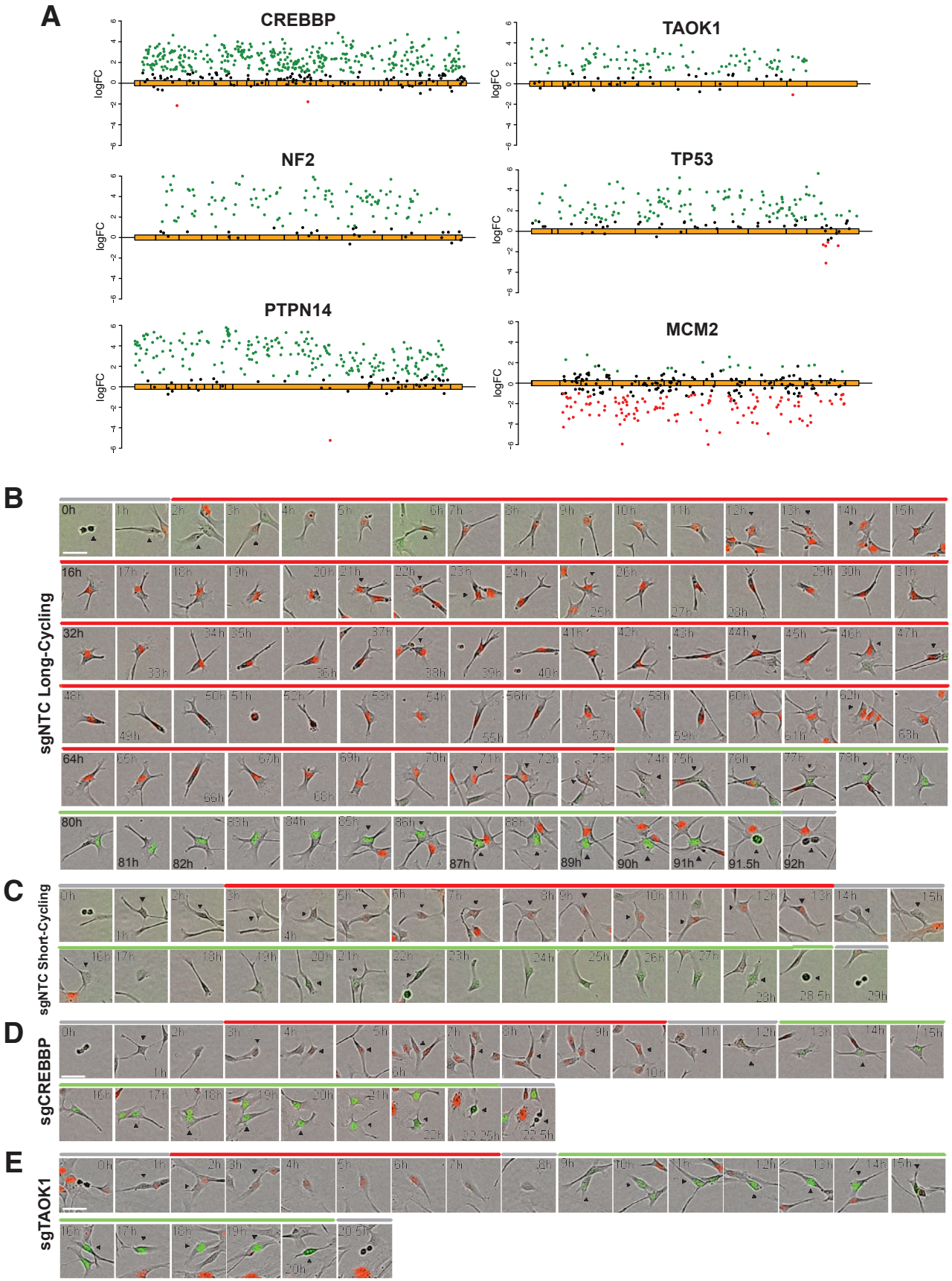
A
CREBBP
TAOK1
NF2
TP53
PTPN14
MCM2
logFC
B
sgNTC Long-Cycling
C
sgNTC Short-Cycling
D
sgCREBBP
E
sgTAOK1

Figure S3 - Transcriptional Target and Cell Cycle Gene Expression Following Loss of G0-skip Genes.

A Hierarchical clustering and percent overlap of differentially expressed up- and down-regulated genes between G0-skip KO and NTC G0/G1 U5-NPCs. Percent gene overlap is relative to the smaller gene set.

B Heat map of high-confidence TP53 target genes (direct regulation score ≥ 10) (Fischer, 2017) that are significantly changed (white dots, FDR<0.05) in at least one G0-skip KO compared to NTC in G0/G1 U5-NPCs measured through RNA-sequencing. The reduction of TP53-dependent transcription is only seen in the TP53 KO.

C Heat map of conserved YAP target genes (Cordenonsi et al., 2011) that are significantly changed (white dots, FDR<0.05) in at least one G0-skip KO compared to NTC in G0/G1 U5-NPCs measured through RNA-sequencing. There are unique subsets of Hippo-YAP target genes up-regulated in NF2 and TAOK1 KOs. Significance of overlap assessed through hypergeometric analysis.

D Venn diagram of YAP target overlap between G0/G1 U5-NPCs with G0-skip KO shows distinct genesets up-regulated by NF2 (sgNF2-YAP) and TAOK1 (sgTAOK1-YAP) KOs as well as some shared targets. PTPN14 KO is most similar to NF2 KO but shares some target up-regulation with TAOK1 KO.

E Gene ontology analysis of the sgNF2-YAP (yellow) and sgTAOK1-YAP (red) target subsets.

F Heat map of the cell cycle genes (Biological process: G0:007049) significantly changed (FDR<0.05) in at least one G0-skip KO compared to NTC in G0/G1 U5-NPCs measured through RNA-sequencing. Subsets that are specifically up- or down-regulated in one or more KO after hierarchical clustering were designated by colored boxes. A subset of corresponding genes were highlighted below in color-corresponding boxes including DREAM complex components down in NF2 KOs (LIN9, MYBL2, and RBL1) and some gene expression changes that were not consistent increased proliferation (i.e., up-regulation of CDK inhibitors CDKN2B/p16 and CDKN2B/p15 in NF2 and PTPN14 KO, up-regulation of CDKN1A/p21 and TP73 in CREBBP KO, and others). In NF2/PTPN14 KO boxes, N=significant in NF2 KO only, P=significant in PTPN14 KO only, and B = significant in both (FDR<0.05 compared to NTC).

All heat maps normalized by read counts per million (CPM) and scale depicts row-wise z-score.

Figure S3

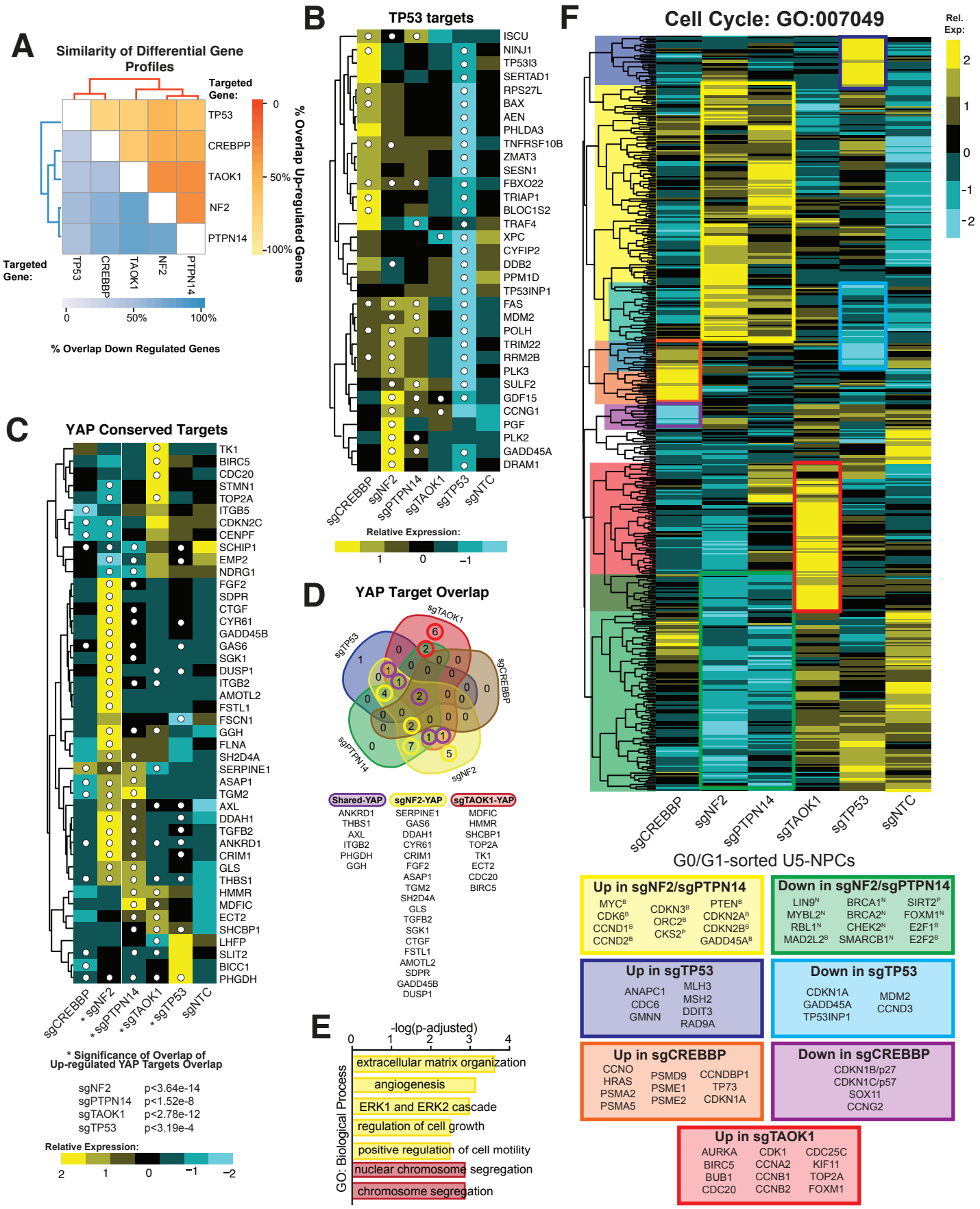
A
Similarity of Differential Gene Profiles
Targeted Gene:
TP53
CREBBP
TAOK1
NF2
PTPN14
% Overlap Up-regulated Genes
0
50%
100%
% Overlap Down Regulated Genes
B
TP53 targets
ISCU
NINJ1
TP53I3
SERTAD1
RPS27L
BAX
AEN
PHLDA3
TNFRSF10B
ZMAT3
SESN1
FBXO22
TRIAP1
BLOC1S2
TRAF4
XPC
CYFIP2
DDB2
PPM1D
TP53INP1
FAS
MDM2
POLH
TRIM22
RRM2B
PLK3
SULF2
GDF15
CCNG1
PGF
PLK2
GADD45A
DRAM1
sgCREBBP
sgNF2
sgPTPN14
sgTAOK1
sgTP53
sgNTC
Relative Expression:
1
0
−1
C
YAP Conserved Targets
TK1
BIRC5
CDC20
STMN1
TOP2A
ITGB5
CDKN2C
CENPF
SCHIP1
EMP2
NDRG1
FGF2
SDPR
CTGF
CYR61
GADD45B
GAS6
SGK1
DUSP1
ITGB2
AMOTL2
FSTL1
FSCN1
GGH
FLNA
SH2D4A
SERPINE1
ASAP1
TGM2
AXL
DDAH1
TGFB2
ANKRD1
CRIM1
GLS
THBS1
HMMR
MDFIC
ECT2
SHCBP1
LHFP
SLIT2
BICC1
PHGDH
sgCREBBP
* sgNF2
* sgPTPN14
* sgTAOK1
* sgTP53
sgNTC
* Significance of Overlap of Up-regulated YAP Targets Overlap
sgNF2 p<3.64e-14
sgPTPN14 p<1.52e-8
sgTAOK1 p<2.78e-12
sgTP53 p<3.19e-4
Relative Expression:
2
1
0
−1
−2
D
YAP Target Overlap
sgTAOK1
sgTP53
sgCREBBP
sgPTPN14
sgNF2
Shared-YAP
ANKRD1
THBS1
AXL
ITGB2
PHGDH
GGH
sgNF2-YAP
SERPINE1
GAS6
DDAH1
CYR61
CRIM1
FGF2
ASAP1
TGM2
SH2D4A
GLS
TGFB2
SGK1
CTGF
FSTL1
AMOTL2
SDPR
GADD45B
DUSP1
sgTAOK1-YAP
MDFIC
HMMR
SHCBP1
TOP2A
TK1
ECT2
CDC20
BIRC5
E
-log(p-adjusted)
0
1
2
3
4
GO: Biological Process
extracellular matrix organization
angiogenesis
ERK1 and ERK2 cascade
regulation of cell growth
positive regulation of cell motility
nuclear chromosome segregation
chromosome segregation
F
Cell Cycle: GO:007049
Rel. Exp:
2
1
0
-1
-2
sgCREBBP
sgNF2
sgPTPN14
sgTAOK1
sgTP53
sgNTC
G0/G1-sorted U5-NPCs
Up in sgNF2/sgPTPN14
MYC^B
CDK6^B
CCND1^B
CCND2^B
CDKN3^B
ORC2^B
CKS2^P
PTEN^B
CDKN2A^B
CDKN2B^B
GADD45A^B
Down in sgNF2/sgPTPN14
LIN9^N
MYBL2^N
RBL1^N
MAD2L2^B
BRCA1^N
BRCA2^N
CHEK2^N
SMARCB1^N
SIRT2^P
FOXM1^N
E2F1^B
E2F2^B
Up in sgTP53
ANAPC1
CDC6
GMNN
MLH3
MSH2
DDIT3
RAD9A
Down in sgTP53
CDKN1A
GADD45A
TP53INP1
MDM2
CCND3
Up in sgCREBBP
CCNO
HRAS
PSMA2
PSMA5
PSMD9
PSME1
PSME2
CCNDBP1
TP73
CDKN1A
Down in sgCREBBP
CDKN1B/p27
CDKN1C/p57
SOX11
CCNG2
Up in sgTAOK1
AURKA
BIRC5
BUB1
CDC20
CDK1
CCNA2
CCNB1
CCNB2
CDC25C
KIF11
TOP2A
FOXM1

Figure S4 - Gene Ontology Analysis of Transcriptional Reprogramming Following Loss of G0-skip Genes.

A,B Dot plot of selected enriched gene ontology (GO) biological processes following G0-skip KO in G0/G1 U5-NPCs for up (A) and down (B) regulated genes compared to NTC. Gene ratio compares the proportion of genes contained within the gene ontology group that are significantly changed in the G0-skip KOs to the total number of genes significantly changed in the G0-skip mutants (either up or down, respectively).

C-E Heat maps for genes (FDR<0.05) defining some of the significant biological process gene ontology groups in G0/G1 U5-NPCs. (C) HIPPO signaling genes (GO:0035329), significantly enriched in NF2 (p-adj.=3.52E-05) or PTPN14 KO (p-adj.=9.42E-05). (D) Mitotic nuclear division genes (GO:007067), significantly enriched in TAOK1 KO (p-adj.=3.16E-10). (E) Respiratory electron transport chain genes (GO:00229004), significantly enriched in CREBBP KO (p-adj.=1.62E-04).

All heat maps normalized to the regularized log (RLD). Scale applies to all heat maps and refers to the row-wise z-score. White dots indicate gene expression significantly different from NTC (FDR<0.05).

Figure S4

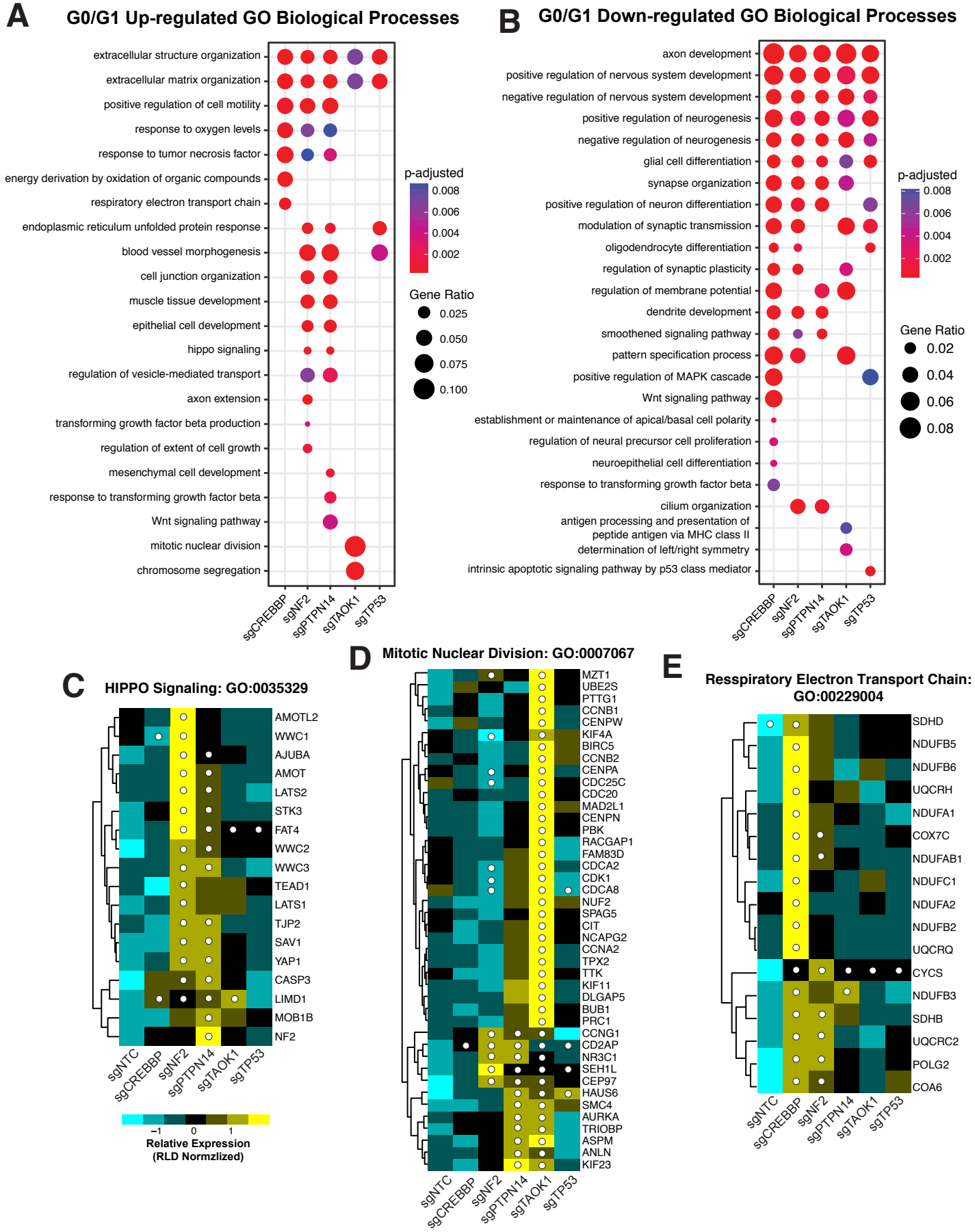
A
G0/G1 Up-regulated GO Biological Processes
extracellular structure organization
extracellular matrix organization
positive regulation of cell motility
response to oxygen levels
response to tumor necrosis factor
energy derivation by oxidation of organic compounds
respiratory electron transport chain
endoplasmic reticulum unfolded protein response
blood vessel morphogenesis
cell junction organization
muscle tissue development
epithelial cell development
hippo signaling
regulation of vesicle-mediated transport
axon extension
transforming growth factor beta production
regulation of extent of cell growth
mesenchymal cell development
response to transforming growth factor beta
Wnt signaling pathway
mitotic nuclear division
chromosome segregation
sgCREBBP
sgNF2
sgPTPN14
sgTAOK1
sgTP53
p-adjusted
0.008
0.006
0.004
0.002
Gene Ratio
0.025
0.050
0.075
0.100
B
G0/G1 Down-regulated GO Biological Processes
axon development
positive regulation of nervous system development
negative regulation of nervous system development
positive regulation of neurogenesis
negative regulation of neurogenesis
glial cell differentiation
synapse organization
positive regulation of neuron differentiation
modulation of synaptic transmission
oligodendrocyte differentiation
regulation of synaptic plasticity
regulation of membrane potential
dendrite development
smoothened signaling pathway
pattern specification process
positive regulation of MAPK cascade
Wnt signaling pathway
establishment or maintenance of apical/basal cell polarity
regulation of neural precursor cell proliferation
neuroepithelial cell differentiation
response to transforming growth factor beta
cilium organization
antigen processing and presentation of peptide antigen via MHC class II
determination of left/right symmetry
intrinsic apoptotic signaling pathway by p53 class mediator
sgCREBBP
sgNF2
sgPTPN14
sgTAOK1
sgTP53
p-adjusted
0.008
0.006
0.004
0.002
Gene Ratio
0.02
0.04
0.06
0.08
C
HIPPO Signaling: GO:0035329
AMOTL2
WWC1
AJUBA
AMOT
LATS2
STK3
FAT4
WWC2
WWC3
TEAD1
LATS1
TJP2
SAV1
YAP1
CASP3
LIMD1
MOB1B
NF2
sgNTC
sgCREBBP
sgNF2
sgPTPN14
sgTAOK1
sgTP53
−1
0
1
Relative Expression
(RLD Normzlized)
D
Mitotic Nuclear Division: GO:0007067
MZT1
UBE2S
PTTG1
CCNB1
CENPW
KIF4A
BIRC5
CCNB2
CENPA
CDC25C
CDC20
MAD2L1
CENPN
PBK
RACGAP1
FAM83D
CDCA2
CDK1
CDCA8
NUF2
SPAG5
CIT
NCAPG2
CCNA2
TPX2
TTK
KIF11
DLGAP5
BUB1
PRC1
CCNG1
CD2AP
NR3C1
SEH1L
CEP97
HAUS6
SMC4
AURKA
TRIOBP
ASPM
ANLN
KIF23
sgNTC
sgCREBBP
sgNF2
sgPTPN14
sgTAOK1
sgTP53
E
Resspiratory Electron Transport Chain:
GO:00229004
SDHD
NDUFB5
NDUFB6
UQCRH
NDUFA1
COX7C
NDUFAB1
NDUFC1
NDUFA2
NDUFB2
UQCRQ
CYCS
NDUFB3
SDHB
UQCRC2
POLG2
COA6
sgNTC
sgCREBBP
sgNF2
sgPTPN14
sgTAOK1
sgTP53

Figure S5 - Identification and Analysis of Cell Cycle Subpopulations from Single Cell RNA-sequencing Unbiased Clustering.

A Number of unique molecular identifiers (nUMI) per cell in each single cell RNA-seq cluster. The Low RNA cluster has dramatically less nUMI than any other cluster, making it difficult to distinguish actual cells belonging to this cluster from background. Therefore, this cluster was excluded from further analysis. The nUMI increases as the cell cycle progresses, with G2/M cells having the greatest nUMI. Significance assessed using a two-tailed student's t-test.

B Comparison of cluster size from scRNA-seq for the entire cell population of U5-NPCs compared to a subpopulation sorted for G0/G1 (mCherry-CDT1(aa30-120)-positive). The clusters with an increase in representation were characterized as G0/G1. Clusters that remained the same or moderately decreased in representation are considered transition states with some of the cells retaining or initiating CDT1 accumulation. Clusters that decreased in representation greater than 2-fold were considered S/G2/M and mCherry-CDT1-negative.

C Dot plot for some of the key markers for each cluster progressing through cell cycle. Color is according to average expression (Avg. Exp.) per cell, while size of the dots corresponds to the proportion of cells within the cluster in which the gene was sequenced (% Exp.). Red text indicates cyclin and cyclin-dependent kinase genes that are differentially expressed in the different clusters. The genes that are depleted in each cluster supports the G0/G1 classification of the cells. For example, *CDK1* is significantly reduced in Neural G0, G1, Late G1, and early G1/M, but enriched in S, S/G2, and G2/M. Similar depletion of other cell cycle genes is seen, including *MKI67* (depleted in Neural G0, late G1, and enriched in G2/M and S/G2, *AURKA* (depleted in Neural G0, G1, S, and M/early G1 and enriched in G2/M), *CCNA2* (depleted in Neural G0, G1, late G1, and M/early G1 and enriched in S/G2 and G2/M), and *TOP2A* (depleted in Neural G0, G1, late G1, and M/early G1 and enriched in S/G2 and G2/M). In addition, Neural G0 showed the most significant repression of these genes peaking in other phases of cell cycle, including suppression of *CCND1* expression.

D Protein-protein interaction networks based on the STRING database (Szklarczyk et al., 2017) for the enriched genes that define the G2/M, S, and S/G2 cluster after single-cell RNA-sequencing in unsorted U5-hNPCs. The thickness of the connecting lines corresponds to the strength of the predicted interaction based on experimental data, curated databases, co-expression analysis, and gene orthology. The network visualization only includes genes that connect with the rest of the network. Genes from enriched gene ontology groups are indicated by colored nodes, including mitotic cell division (red), DNA replication (purple), DNA conformation change (yellow), and RNA-related genes from various gene ontology biological processes (green).

Figure S5

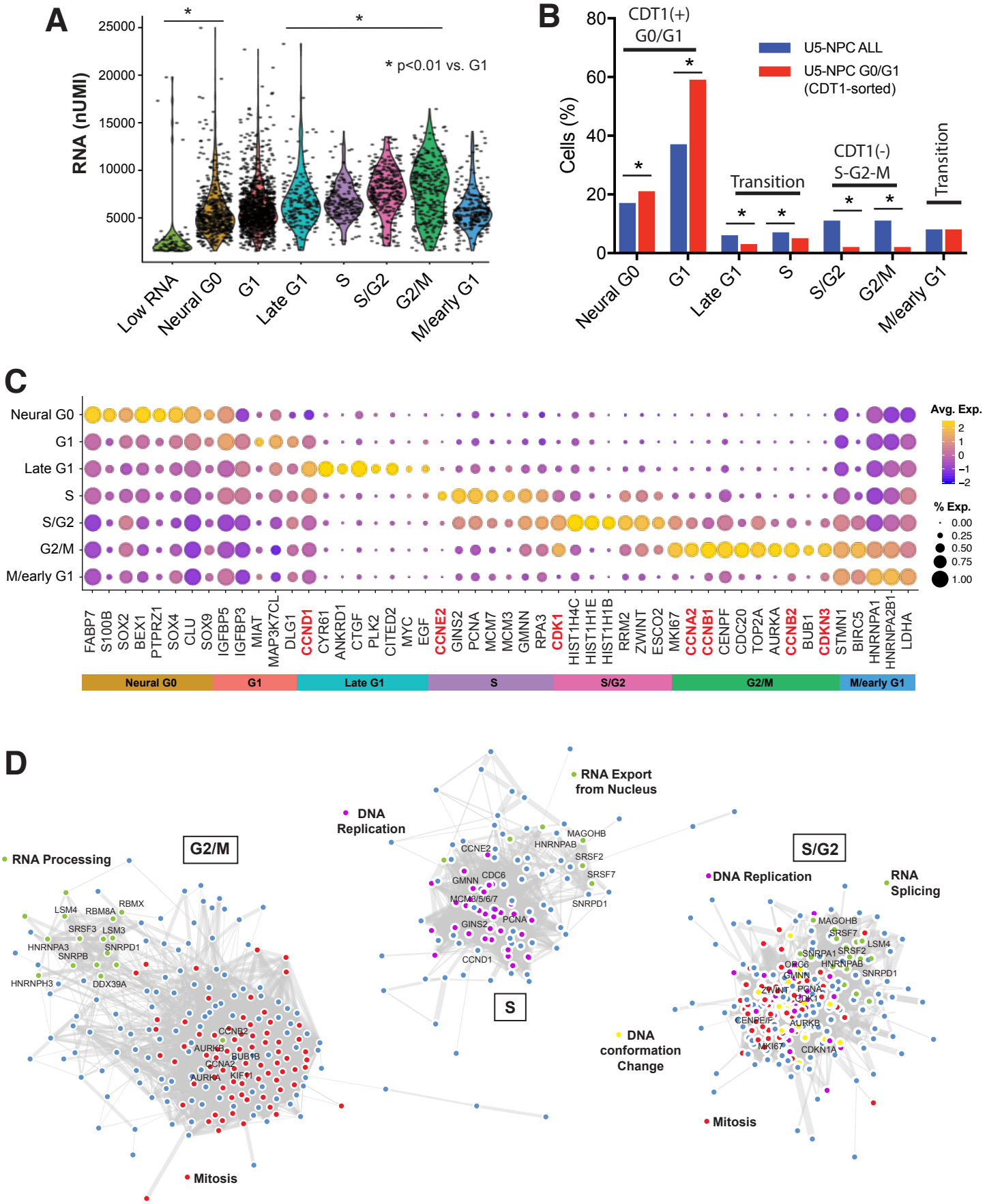
A
RNA (nUMI)
25000
20000
15000
10000
5000
* p<0.01 vs. G1
Low RNA
Neural G0
G1
Late G1
S
S/G2
G2/M
M/early G1
B
Cells (%)
80
60
40
20
0
CDT1(+) G0/G1
U5-NPC ALL
U5-NPC G0/G1 (CDT1-sorted)
Transition
CDT1(-) S-G2-M
Transition
C
Neural G0
G1
Late G1
S
S/G2
G2/M
M/early G1
Avg. Exp.
% Exp.
0.00
0.25
0.50
0.75
1.00
FABP7 S100B SOX2 BEX1 PTPRZ1 SOX4 CLU SOX9 IGFBP5 IGFBP3 MIAT MAP3K7CL DLG1 CCND1 CYR61 ANKRD1 CTGF PLK2 CITED2 MYC EGF CCNE2 GINS2 PCNA MCM7 MCM3 GMNN RPA3 CDK1 HIST1H4C HIST1H1E HIST1H1B RRM2 ZWINT ESCO2 MKI67 CCNA2 CCNB1 CENPF CDC20 TOP2A AURKA CCNB2 BUB1 CDKN3 STMN1 BIRC5 HNRNPA1 HNRNPA2B1 LDHA
D
G2/M
RNA Processing
Mitosis
DNA Replication
RNA Export from Nucleus
S
S/G2
DNA Replication
RNA Splicing
DNA conformation Change
Mitosis

Figure S6 - Further Analysis of Cell Cycle Subpopulations from Single Cell RNA-sequencing and Comparison to Other Datasets.

A Protein-protein interaction networks based on the STRING database (Szklarczyk et al., 2017) for the enriched genes that define the G0/G1 clusters: Neural G0, Early G1/M and Late G1. The network visualization only includes genes that connect with the rest of the network. G1 only showed enriched interactions between IGFR1 signaling genes IGFBP3 and IGFBP5 (not visualized). Neural G0 has a more diffuse network with only a few interactions per gene and includes a number of transcription factors that may be important in mediating this cell cycle state (pink). The late G1 cluster has two gene groups: the cholesterol synthesis group (orange) and YAP-NF2 targets (yellow). M/early G1 retains residual expression or non-degradation of a subset of genes enriched in G2/M, including the mitosis-peaking genes CCNB2, CDKN3, and BIRC5 (red) as well as spliceosomal genes (green).

B Overlap of conserved YAP target genes up-regulated following G0-skip knockout of NF2 (yellow), TAOK1 (red), or both (purple) (see Fig S3C) with genes defining cell cycle transcriptional clusters. The NF2-dependent YAP targets significantly overlap with the Late G1 cluster, while the TAOK1-dependent genes overlap with the S/G2 and G2/M clusters. Significance assessed using hypergeometric analysis.

C Proportion of mouse embryonic stem cells (mESCs) (Buettner et al., 2015) classified to each hNPC transcriptional cluster following sorting for cell cycle by Hoechst staining for amount of DNA.

D Significance of overlap of the neurogenesis cell subpopulation-defining genes in the early neurogenic lineage from two murine single cell RNA-sequencing studies (Artegiani et al., 2017, Llorens-Bobadilla et al., 2015) compared to single cell cluster definitions (up-regulated genes) from unsorted U5-hNPCs grown in culture. Clusters presented in order of increasing activation with quiescent neural stem cells on the left and proliferating progenitors on the right. Significance assessed though hypergeometric analysis. RF = representation factor. NSC = neural stem cell. OPC = oligodendrocyte progenitor. q = quiescent. a = activated.

Figure S6

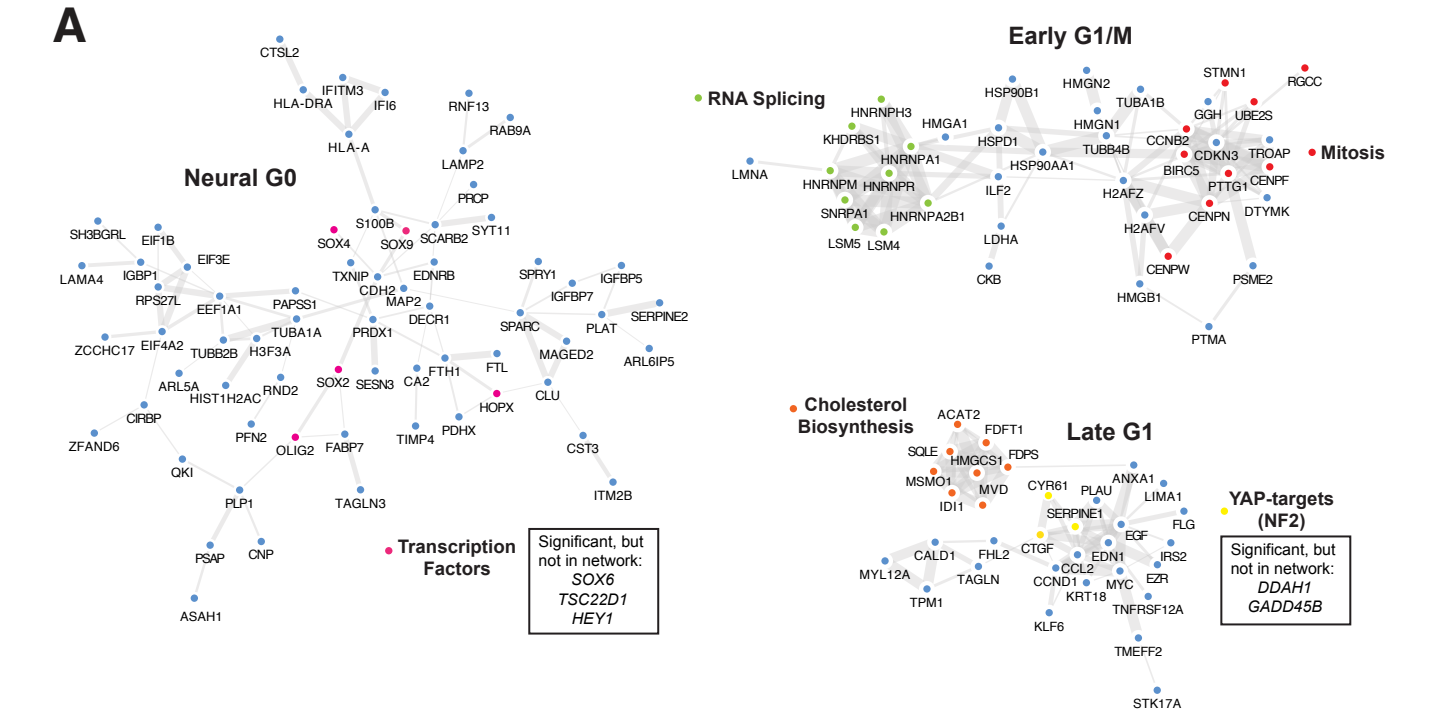
A
Neural G0
CTSL2
IFITM3
HLA-DRA
IFI6
RNF13
RAB9A
HLA-A
LAMP2
PRCP
S100B
SOX4
SOX9
SCARB2
SYT11
SH3BGRL
EIF1B
EIF3E
LAMA4
IGBP1
RPS27L
EEF1A1
PAPSS1
TXNIP
CDH2
EDNRB
MAP2
DECR1
TUBA1A
PRDX1
ZCCHC17
EIF4A2
TUBB2B
H3F3A
ARL5A
HIST1H2AC
RND2
SOX2
SESN3
CA2
FTH1
FTL
SPRY1
IGFBP5
IGFBP7
SERPINE2
SPARC
PLAT
MAGED2
ARL6IP5
HOPX
CLU
CIRBP
ZFAND6
PFN2
OLIG2
FABP7
TIMP4
PDHX
CST3
QKI
PLP1
TAGLN3
ITM2B
PSAP
CNP
ASAH1
Transcription Factors
Significant, but not in network:
SOX6
TSC22D1
HEY1
Early G1/M
RNA Splicing
HNRNPH3
HMGA1
KHDRBS1
HNRNPA1
LMNA
HNRNPM
HNRNPR
SNRPA1
HNRNPA2B1
LSM5
LSM4
HSP90B1
HSPD1
HSP90AA1
ILF2
LDHA
CKB
HMGN2
HMGN1
TUBA1B
TUBB4B
H2AFZ
H2AFV
STMN1
RGCC
GGH
UBE2S
CCNB2
CDKN3
TROAP
BIRC5
PTTG1
CENPF
CENPN
DTYMK
CENPW
PSME2
HMGB1
PTMA
Mitosis
Cholesterol Biosynthesis
ACAT2
FDFT1
SQLE
HMGCS1
FDPS
MSMO1
IDI1
MVD
Late G1
CYR61
PLAU
ANXA1
LIMA1
SERPINE1
FLG
EGF
CTGF
EDN1
IRS2
CCL2
CCND1
MYC
EZR
KRT18
TNFRSF12A
KLF6
TMEFF2
STK17A
CALD1
FHL2
MYL12A
TAGLN
TPM1
YAP-targets (NF2)
Significant, but not in network:
DDAH1
GADD45B

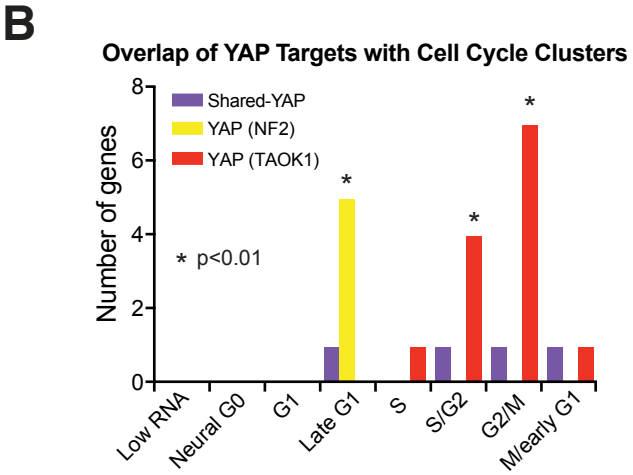
B
Overlap of YAP Targets with Cell Cycle Clusters
Number of genes
Shared-YAP
YAP (NF2)
YAP (TAOK1)
* p<0.01
Low RNA
Neural G0
G1
Late G1
S
S/G2
G2/M
M/early G1

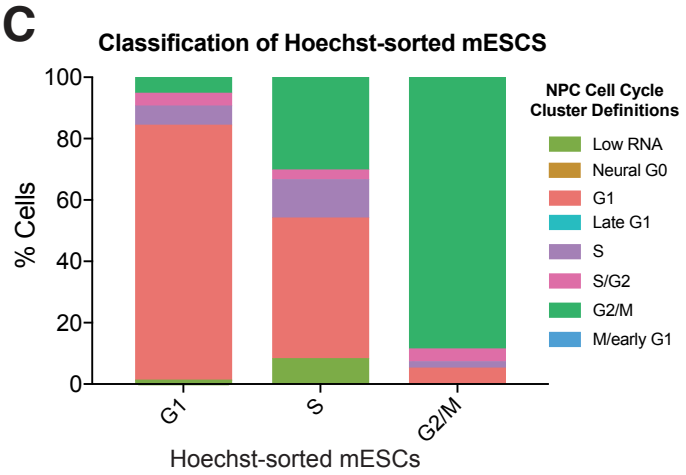
C
Classification of Hoechst-sorted mESCS
% Cells
NPC Cell Cycle Cluster Definitions
Low RNA
Neural G0
G1
Late G1
S
S/G2
G2/M
M/early G1
Hoechst-sorted mESCs

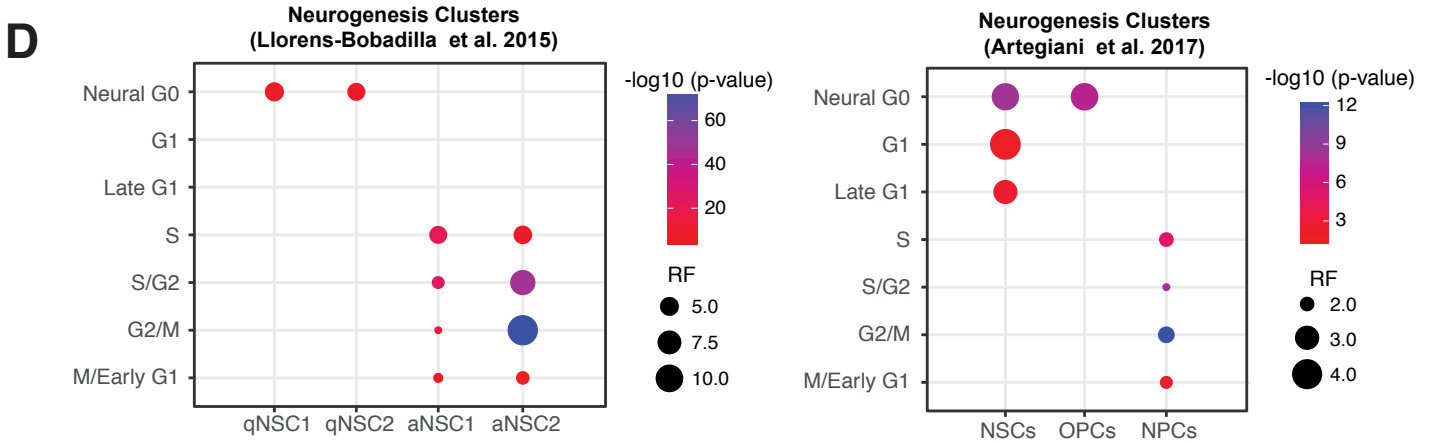
D
Neurogenesis Clusters
(Llorens-Bobadilla et al. 2015)
Neural G0
G1
Late G1
S
S/G2
G2/M
M/Early G1
qNSC1
qNSC2
aNSC1
aNSC2
-log10 (p-value)
RF
Neurogenesis Clusters
(Artegiani et al. 2017)
NSCs
OPCs
NPCs

Figure S7 - Altered Expression of Single-Cell Cell Cycle Cluster Definition Genes in RNA-sequencing Datasets and Differentiation in G0-skip Mutants.

A,B Overlap of genes that are significantly down (A) or up (B) following G0-skip KO in G0/G1 U5-NPCs compared to the Neural G0 (A) or Late G1 (B) single cell RNA-sequencing clusters.
C,D Significance of overlap of the down (C) and up (D) regulated genes from bulk RNA-sequencing of G0/G1 sorted 0131 and 0827 glioblastoma stem cell (GSC) isolates with the single cell cluster definitions (up-regulated genes). Significance assessed though hypergeometric analysis. RF = representation factor.
E Immunocytochemistry of U5-NPCs in normal NPC culture conditions and after 1 week removal of growth factors (GF) (EGF and FGF withdrawal). Staining is for various neural lineage markers including the neural stem/progenitor markers Nestin (green) and Sox2 (red), the glial marker GFAP (red), and the neuronal marker beta-tubulin III (TUJ1; green). Scale bar = 50 μm.
F Dendrogram of unbiased hierarchical clustering of gene expression from U5-NPCs before and after 1 week of growth factor withdrawal (controls) and after KO of G0-skip genes.
G Venn diagram for brain-specific transcription factors (Gray et al., 2004) that are significantly reduced (FDR<0.05) in G0-skip mutants compared to NTC following 1 week differentiation through growth factor-withdrawal. Bold indicates the transcription factor that is reduced in all G0-skip mutants, FOXJ1.
H Gene expression of GFAP (glial marker) and DRC1 (cilia component) before (NPC) and after 1 week of mitogenic GF withdrawal (diff) for control cells and after KO of G0-skip genes. These genes are significantly induced during differentiation and reduced in the G0-skip mutants to varying degrees.

Figure S7

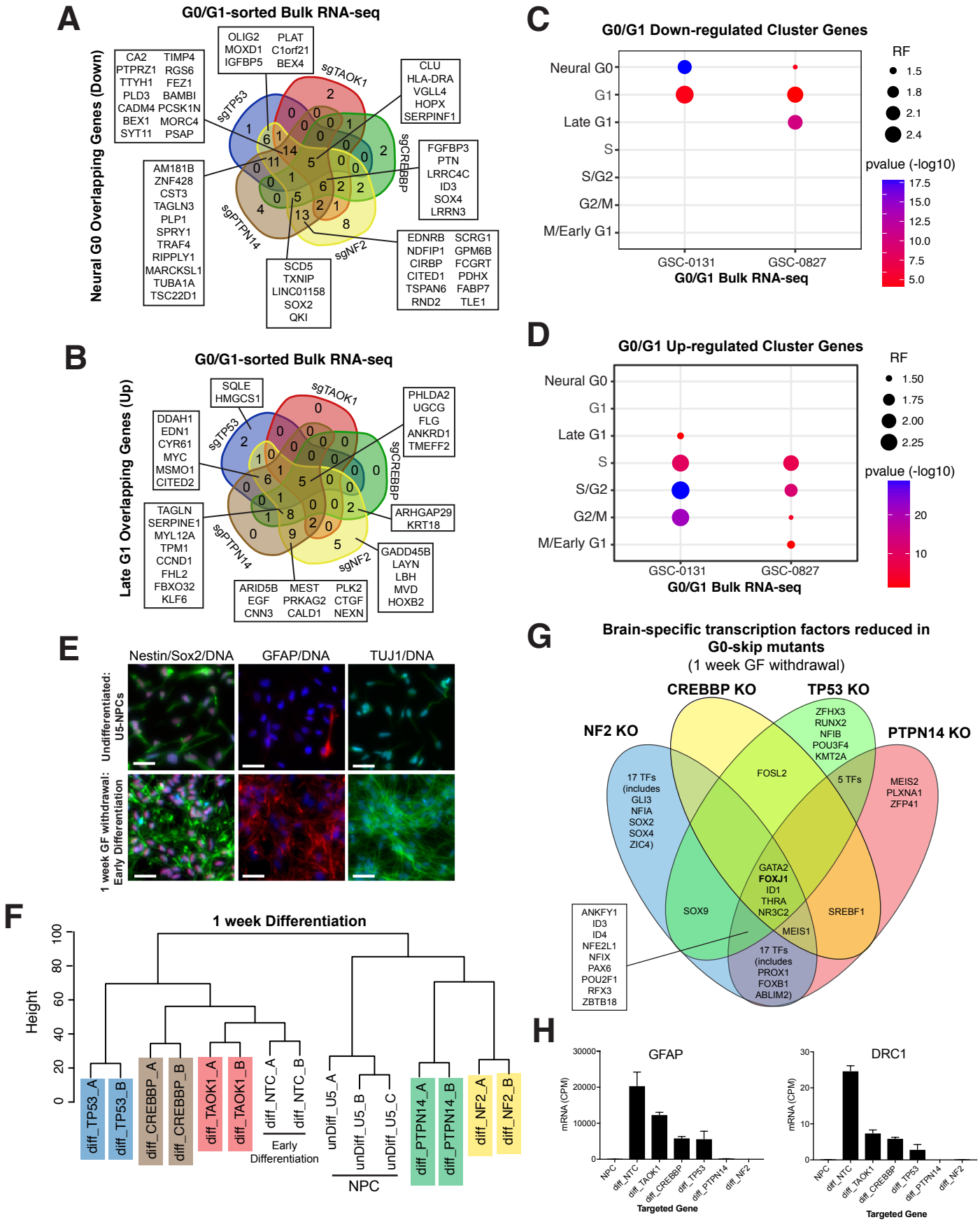
A
G0/G1-sorted Bulk RNA-seq
Neural G0 Overlapping Genes (Down)
sgTP53
sgTAOK1
sgCREBBP
sgPTPN14
sgNF2
CA2 TIMP4 PTPRZ1 RGS6 TTYH1 FEZ1 PLD3 BAMBI CADM4 PCSK1N BEX1 MORC4 SYT11 PSAP
OLIG2 PLAT MOXD1 C1orf21 IGFBP5 BEX4
CLU HLA-DRA VGLL4 HOPX SERPINF1
FGFBP3 PTN LRRC4C ID3 SOX4 LRRN3
AM181B ZNF428 CST3 TAGLN3 PLP1 SPRY1 TRAF4 RIPPLY1 MARCKSL1 TUBA1A TSC22D1
EDNRB SCRG1 NDFIP1 GPM6B CIRBP FCGRT CITED1 PDHX TSPAN6 FABP7 RND2 TLE1
SCD5 TXNIP LINC01158 SOX2 QKI
B
G0/G1-sorted Bulk RNA-seq
Late G1 Overlapping Genes (Up)
sgTP53
sgTAOK1
sgCREBBP
sgPTPN14
sgNF2
SQLE HMGCS1
DDAH1 EDN1 CYR61 MYC MSMO1 CITED2
PHLDA2 UGCG FLG ANKRD1 TMEFF2
TAGLN SERPINE1 MYL12A TPM1 CCND1 FHL2 FBXO32 KLF6
ARHGAP29 KRT18
GADD45B LAYN LBH MVD HOXB2
ARID5B MEST PLK2 EGF PRKAG2 CTGF CNN3 CALD1 NEXN
C
G0/G1 Down-regulated Cluster Genes
Neural G0
G1
Late G1
S
S/G2
G2/M
M/Early G1
GSC-0131
GSC-0827
G0/G1 Bulk RNA-seq
RF
1.5
1.8
2.1
2.4
pvalue (-log10)
17.5
15.0
12.5
10.0
7.5
5.0
D
G0/G1 Up-regulated Cluster Genes
Neural G0
G1
Late G1
S
S/G2
G2/M
M/Early G1
GSC-0131
GSC-0827
G0/G1 Bulk RNA-seq
RF
1.50
1.75
2.00
2.25
pvalue (-log10)
20
10
E
Nestin/Sox2/DNA
GFAP/DNA
TUJ1/DNA
Undifferentiated: U5-NPCs
1 week GF withdrawal: Early Differentiation
F
1 week Differentiation
Height
0
20
40
60
80
100
diff_TP53_A
diff_TP53_B
diff_CREBBP_A
diff_CREBBP_B
diff_TAOK1_A
diff_TAOK1_B
diff_NTC_A
diff_NTC_B
Early Differentiation
unDiff_U5_A
unDiff_U5_B
unDiff_U5_C
NPC
diff_PTPN14_A
diff_PTPN14_B
diff_NF2_A
diff_NF2_B
G
Brain-specific transcription factors reduced in G0-skip mutants
(1 week GF withdrawal)
CREBBP KO
TP53 KO
NF2 KO
PTPN14 KO
17 TFs (includes GLI3 NFIA SOX2 SOX4 ZIC4)
FOSL2
ZFHX3 RUNX2 NFIB POU3F4 KMT2A
5 TFs
MEIS2 PLXNA1 ZFP41
GATA2 FOXJ1 ID1 THRA NR3C2
SOX9
SREBF1
MEIS1
17 TFs (includes PROX1 FOXB1 ABLIM2)
ANKFY1 ID3 ID4 NFE2L1 NFIX PAX6 POU2F1 RFX3 ZBTB18
H
GFAP
mRNA (CPM)
30000
20000
10000
0
NPC
diff_NTC
diff_TAOK1
diff_CREBBP
diff_TP53
diff_PTPN14
diff_NF2
Targeted Gene
DRC1
mRNA (CPM)
30
20
10
0
NPC
diff_NTC
diff_TAOK1
diff_CREBBP
diff_TP53
diff_PTPN14
diff_NF2
Targeted Gene